ARTICLE
PUBLISHED ONLINE: 14 NOVEMBER 2016 | DOI: 10.1038/NCHEMBIO.2238

Oxidized arachidonic and adrenic PEs navigate cells to ferroptosis

Valerian E Kagan[1–4]*, Gao+wei Mao[1,5,13], Feng Qu[1,13], Jose Pedro Friedmann Angeli[6,13], Sebastian Doll[6], Claudette St Croix[7], Haider Hussain Dar[1], Bing Liu[8], Vladimir A Tyurin[1], Vladimir B Ritov[1], Alexandr A Kapralov[1], Andrew A Amoscato[1], Jianfei Jiang[1], Tamil Anthonymuthu[5], Dariush Mohammadyani[1], Qin Yang[5], Bettina Proneth[6], Judith Klein-Seetharaman[9], Simon Watkins[7], Ivet Bahar[8], Joel Greenberger[4], Rama K Mallampalli[10], Brent R Stockwell[11,12], Yulia Y Tyurina[1], Marcus Conrad[6]* & Hülya Bayır[1,5]*

Enigmatic lipid peroxidation products have been claimed as the proximate executioners of ferroptosis—a specialized death program triggered by insufficiency of glutathione peroxidase 4 (GPX4). Using quantitative redox lipidomics, reverse genetics, bioinformatics and systems biology, we discovered that ferroptosis involves a highly organized oxygenation center, wherein oxidation in endoplasmic-reticulum-associated compartments occurs on only one class of phospholipids (phosphatidylethanolamines (PEs)) and is specific toward two fatty acyls—arachidonoyl (AA) and adrenoyl (AdA). Suppression of AA or AdA esterification into PE by genetic or pharmacological inhibition of acyl-CoA synthase 4 (ACSL4) acts as a specific antiferroptotic rescue pathway. Lipoxygenase (LOX) generates doubly and triply-oxygenated (15-hydroperoxy)-diacylated PE species, which act as death signals, and tocopherols and tocotrienols (vitamin E) suppress LOX and protect against ferroptosis, suggesting a homeostatic physiological role for vitamin E. This oxidative PE death pathway may also represent a target for drug discovery.

Multicellular eukaryotes have death programs to optimize tissue homeostasis, immune and stress responses and embryogenesis[1]. Such programs are also beneficial for unicellular eukaryotes and—through quorum sensing—for bacteria, thus making cell death paradoxically essential for all kingdoms of life. On a global scale, redox ferro–ferric cycling of iron by microorganisms controls the fate of this element in the environment[2]. In eukaryotic cells, the electron donor–acceptor propensities that define the vital role of iron in normal physiology facilitate the ferroptotic death program[3,4].

Ferroptosis is switched on by the dysregulation of one of the two major redox systems—thiol or lipid peroxidation, whereby a combination of GPX4 or glutathione (GSH) deficiency and activation of one or more putative iron-containing enzymes generates oxygenated lipids as the proximal signals of death[5]. However, neither direct evidence for lipid peroxidation nor the nature of the oxygenated lipid species responsible for the ferroptotic cell demise has been established. Here, we established that LOX, among other iron-containing sources of oxidation, can directly oxidize AA- and AdA-PE into ferroptotic signals, and that this process is facilitated by ACSL4-driven esterification of AA and AdA into PE.

RESULTS

Lipid hydroperoxides accumulate in ferroptotic ER

To induce GPX4 deficiency in mouse embryonic fibroblasts (Pfa1), we used RSL3, a potent and selective GPX4 inhibitor[6]. RSL3 triggered ferroptotic death (**Supplementary Results**, **Supplementary Fig. 1a**) and caused a marked decrease in activity of GPX4 (**Supplementary Fig. 1b**). After chemical inactivation by RSL3, we observed a marked decrease in abundance of GPX4 (**Supplementary Fig. 1c**), suggesting that GPX4 activity is needed to prevent its instability or degradation.

GPX4 catalyzes the reduction of phospholipid hydroperoxides and neutral lipid hydroperoxides to their respective hydroxy derivatives[7]. We endeavored to detect the formation of lipid hydroperoxides in GPX4-deficient Pfa1 cells. We employed live cell imaging with LiperFluo, which, similarly to GPX4, reduces lipid hydroperoxides to their hydroxy homologs to yield a fluorescent product[8]. We observed a robust and time-dependent fluorescent LiperFluo response (**Fig. 1a**,**b**) that preceded RSL3-triggered ferroptotic death of wild-type (WT) Pfa1 cells (**Fig. 1c**). Accumulation of LiperFluo-reactive lipid hydroperoxides occurred extramitochondrially, predominantly in the endoplasmic reticulum (ER) compartment (**Fig. 1d**).

Measurements of reactive oxygen species (ROS) and pro-oxidant activity toward nonlipidic fluorogenic substrates (for example, a lipid ROS probe, C11-BODIPY or linoleamide alkyne click-conjugated by cyclo-addition reaction with fluorescein azide) have been used as surrogate measures for lipid peroxidation[9]. Although fluorescence responses from these probes showed overall activation during ferroptosis, they could not reveal the direct production of lipid hydroperoxides. Both C11-BODIPY and LiperFluo

[1]Department of Environmental and Occupational Health, University of Pittsburgh, Pittsburgh, Pennsylvania, USA. [2]Department of Pharmacology and Chemical Biology, University of Pittsburgh, Pittsburgh, Pennsylvania, USA. [3]Department of Chemistry, University of Pittsburgh, Pittsburgh, Pennsylvania, USA. [4]Department of Radiation Oncology, University of Pittsburgh, Pittsburgh, Pennsylvania, USA. [5]Department of Critical Care Medicine, University of Pittsburgh, Pittsburgh, Pennsylvania, USA. [6]Institute of Developmental Genetics, Helmholtz Zentrum München, Neuherberg, Germany. [7]Department of Cell Biology, University of Pittsburgh, Pittsburgh, Pennsylvania, USA. [8]Department of Computational and Systems Biology, University of Pittsburgh, Pittsburgh, Pennsylvania, USA. [9]Division of Metabolic and Vascular Health, University of Warwick, Coventry, UK. [10]Department of Medicine, University of Pittsburgh, Pittsburgh, Pennsylvania, USA. [11]Department of Biological Sciences, Columbia University, New York, New York, USA. [12]Department of Chemistry, Columbia University, New York, New York, USA. [13]These authors contributed equally to this work. *e-mail: kagan@pitt.edu, marcus.conrad@helmholtz-muenchen.de or bayihx@ccm.upmc.edu

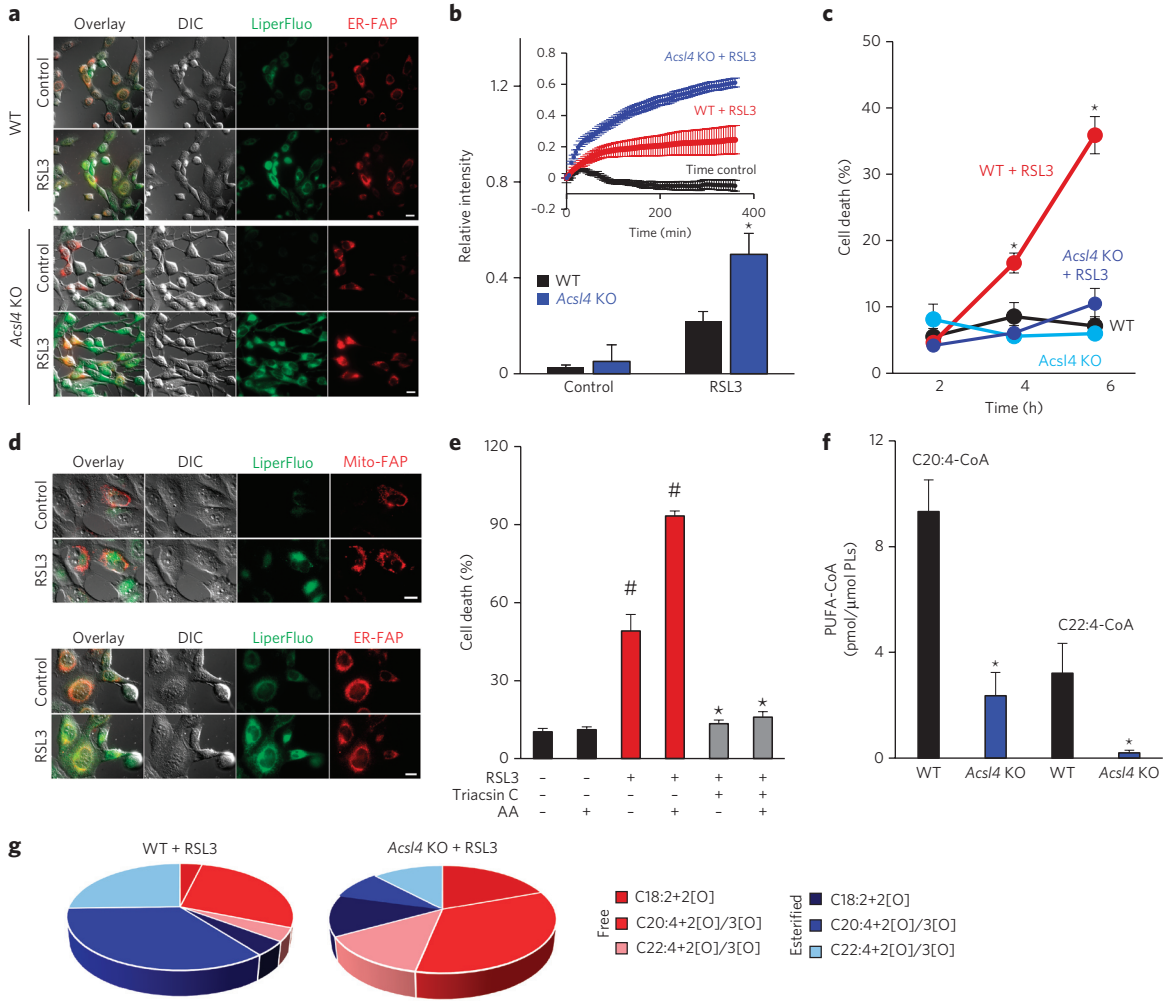

Figure 1 | Oxygenation of esterified AA contributes to RSL3-induced ferroptosis in WT and *Acsl4* KO Pfa1 cells. (**a**) Live cell fluorescence imaging of lipid hydroperoxides in WT and *Acsl4* KO cells treated with RSL3 (100 nM, 6 h). DIC, differential interference contrast; ER-FAP, ER-targeted fluorogen-activating protein. Scale bars, 5 µm. (**b**) LiperFluo fluorescence intensity (relative to baseline) after RSL3 treatment in WT and *Acsl4* KO cells. Control, no RSL3 treatment. Inset, fluorescence time course after RSL3 treatment (100 nM) in WT and *Acsl4* KO cells with a time control. Data are from a minimum of 10 stage positions. For statistical analysis, each stage position counted as one data entry. Data are mean ± s.d., $^*P < 0.05$ (*t*-test). (**c**) Cell death in WT and *Acsl4* KO cells treated with RSL3 (100 nM) for 2, 4 or 6 h before analysis. Data are mean ± s.d., $n = 3$ samples per group. $^*P < 0.05$ (*t*-test). (**d**) Fluorescence responses in pfa1 cells from mitochondrially targeted fluorogen-activating protein (mito-FAP, top) and ER-FAP (bottom) versus LiperFluo. Scale bars, 5 µm. (**e**) Ferroptosis in Pfa1 cells treated with triacsin C (2.5 µM, 6 h), AA (2.5 µM, 16 h) and/or RSL3 (100 nM, 6 h) as indicated. Data are mean ± s.d., $n = 3$. $^*P < 0.05$ (*t*-test), $^{\#}P < 0.05$ (*t*-test). (**f**) AA-CoA and AdA-CoA contents in WT and *Acsl4* KO cells. Data are mean ± s.d., $n = 3$. $^*P < 0.05$ (*t*-test). (**g**) Distribution of free and esterified PUFA-OOH in WT and *Acsl4* KO Pfa1 cells treated with RSL3 (100 nM, 6 h). Results from at least biological triplicates are presented unless otherwise specified.

can react with peroxyl radicals, whereas LiperFluo (but not C11-BODIPY) interacts with (phospho)lipid hydroperoxides[10]. By contrast, LiperFluo fluorescence reliably reports intracellular sites of lipid hydroperoxide accumulation[8].

GPX4 reduces hydroperoxides of polyunsaturated fatty acids (PUFA-OOH) and phospholipids (PL-OOH)[7]. Esterification of PUFA into phospholipids requires acyl-CoA synthase–catalyzed formation of PUFA-CoA. Specifically, ACSL4 catalyzes synthesis of long-chain polyunsaturated CoAs with a preference for AA[11], thus facilitating their esterification into phospholipids[12]. Genetic ablation[13] and inhibition of ACSL4 by triacsin C were effective in protecting against RSL3-induced cell death (**Fig. 1e**). However, we found a more robust LiperFluo fluorescence response from *Acsl4* knockout (KO) cells compared to WT cells (**Fig. 1a**,**b**). Because *Acsl4* KO cells showed decreased levels of polyunsaturated-acyl-CoAs (**Fig. 1f**), they probably accumulate free PUFA-OOH (rather than esterified PL-OOH), causing elevated fluorescence emission. To test this, we performed LC-MS/MS analysis of free PUFA-OOH and PL-OOH in WT and *Acsl4* KO cells. We used platelet-activating factor acetylhydrolase (PAF-AH), which specifically cleaves the oxidized PUFA residues from phospholipids[14] to yield FA-OOH and lysophospholipids. In *Acsl4* KO cells, RSL3 predominantly induced accumulation of free oxygenated PUFA (**Fig. 1g**), whereas WT cells showed higher levels of esterified oxygenated AA (C20:4) and AdA (C22:4) (**Fig. 1g**). Assessments of the reaction rate constants with LiperFluo in ethanol showed that its reactivity toward free PUFA-OOH was slightly higher than that with PL-OOH (reaction rate constants of $1.6 \pm 0.1 \times 10^3$ $M^{-1}s^{-1}$ (ref. 15) and $1.2 \pm 0.1 \times 10^3$ $M^{-1}s^{-1}$, respectively). Thus, higher contents of free PUFA-OOH and its higher reactivity toward LiperFluo both contributed to the robust fluorescence response to LiperFluo in *Ascl4* KO cells.

AA enhances ferroptotic response in RSL3-treated cells

To investigate whether esterified oxygenated PUFA acts as the proximate executioner of ferroptotic death, we supplemented WT and *Acsl4* KO cells with exogenous AA. This resulted in a 24% increase

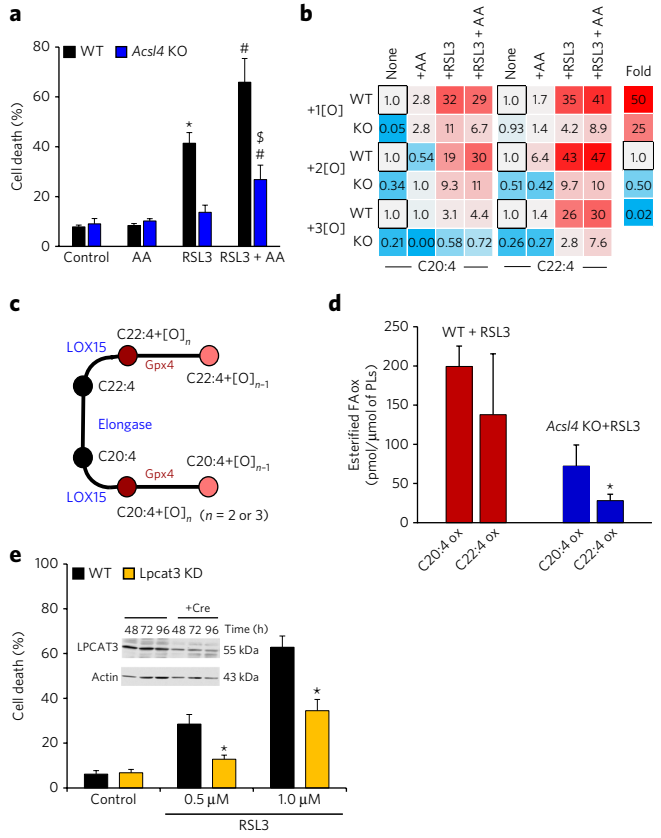

Figure 2 | Effects of exogenous AA on RSL3-triggered ferroptosis. (**a**) Cell death in WT and *Acsl4* KO cells treated with AA (2.5 μM, 16 h) followed by RSL3 (100 nM, 6 h). Control, no AA or RSL3 treatment. Data are mean ± s.d., $n = 3$; $^*P$, $^{\#}P$ and $^{\$}P < 0.05$ versus control, RSL3 and RSL3+AA, respectively (*t*-test). (**b**) LC-MS-based heat maps showing relative changes in oxygenated esterified AA (C20:4) and AdA (C22:4) (normalized to corresponding WT group) after different treatments. (**c**) Metabolic pathways for C20:4, C22:4 and their oxygenated products. (**d**) Levels of oxidized C20:4 (C20:4 ox) and oxidized C22:4 (C22:4ox) esterified into phospholipids (FAox) in WT and *Acsl4* KO Pfa1 cells. Data are mean ± s.e.m., $n = 3$. $^*P < 0.05$ versus WT cells (one-tailed *t*-test). (**e**) Decreased RSL3-induced ferroptosis after *Lpcat3* knockdown (KD) in MLE cells. Inset, LPCAT3 decrease confirmed by western blotting (48, 72 and 96 h) after activation of shRNA against Lpcat3 by Cre addition (for the full blot, see **Supplementary Fig. 18a**). Data are mean ± s.d., $n = 3$. $^*P < 0.05$ versus WT cells (*t*-test). Results from at least biological triplicates are presented unless otherwise specified.

in ferroptosis in RSL3-treated WT cells, compared to a 13% increase in cell death in *Acsl4* KO cells (**Fig. 2a**). Accordingly, LC-MS/MS analysis (after PAF-AH treatment) showed greater accumulation of esterified oxygenated AA in phospholipids of WT than in *Acsl4* KO cells after RSL3 treatment (**Fig. 1g**). Additionally, we observed that supplementation with AA triggered elongation activity, resulting in increased amounts of AdA and its oxygenated forms (**Fig. 2b,c**). The amounts of oxygenated esterified AA and AdA were lower in RSL3-treated *Acsl4* KO cells than in RSL3-treated WT cells (72.2 ± 27.0 and 28.2 ± 8.0, compared to 199.3 ± 26.2 and 137.8 ± 77.7 pmol/μmol phospholipids, respectively, $P < 0.01$) (**Fig. 2d**).

Remodeling of phospholipids via the reacylation (Lands) cycle requires insertion of an acyl group into lysophospholipid, an enzymatic step catalyzed by lysophosphatidylcholine acyltransferase 3 (LPCAT3), which is specific toward long-chain phosphatidylcholine (PC)- and PE-based substrates. We found that knockdown of *Lpcat3* increased resistance to ferroptosis triggered by RSL3 in mouse lung epithelial (MLE) cells (**Fig. 2e**) and mouse embryonic cells (**Supplementary Fig. 1d**), and these results are in line with a previous report[16].

Redox phospholipidomics of ferroptotic signals

Among the eight distinct isoforms of GSH peroxidases, only GPX4 can reduce PL-OOH in membranes. To identify the proferroptotic oxygenated phospholipids, we performed global redox phospholipidomics LC-MS/MS analysis of RSL3-treated WT and *Acsl4* KO Pfa1 cells, *Gpx4* KO Pfa1 cells and kidney cells from *Gpx4* KO mice. Overall, we detected 350 individual species of phospholipids in five major classes—PC, PE, phosphatidylserine (PS), phosphatidylglycerol (PG), phosphatidylinositol (PI) and cardiolipin (CL)—in Pfa1 cells (**Fig. 3a**). This included 220 nonoxygenated and 130 oxygenated phospholipid species. Oxygenated derivatives with different numbers of oxygen atoms were found in all these major classes of phospholipids, with the exception of CL (**Fig. 3b** and **Supplementary Fig. 2a**). Most oxygenated phospholipids showed a trend toward increased levels in ferroptotic cells but differed from one another in terms of fold increase and the significance of the changes. Therefore, we used these two features to rank oxygenated phospholipids by likelihood of being lipid death signals (**Fig. 3b,c**). We applied a series of quantitative inclusion criteria (**Supplementary Fig. 3**): (i) ≥3-fold increase in content in ferroptotic versus control cells ($P < 0.05$); (ii) $R > 0.7$ for correlation with cell death; (iii) reduced levels of nonoxygenated oxidizable precursors in *Acsl4* KO cells; and (iv) elevated levels in *Gpx4* KO cells *in vitro* and *Gpx4* KO mice *in vivo*. Sequential application of these criteria reduced the number of candidates from 110 to 44, then to 17 (**Supplementary Table 1**), 8 and finally 4 (**Fig. 3d** and **Supplementary Fig. 2b,c**). These four remaining molecular species were all doubly and triply oxygenated PEs.

Oxygenated PE in *Gpx4* KO cells and kidney

In a model of genetic depletion of GPX4, we observed that death in *Gpx4* KO cells (**Supplementary Fig. 4**)[17] was accompanied by elevated levels of doubly and triply oxygenated AA- and AdA-containing PE species (**Fig. 4a–c**). We previously found that depletion of GPX4 *in vivo* causes acute renal failure, accumulation of oxygenated phospholipids and ferroptosis[18]. LC-MS analysis revealed accumulation of ten oxygenated PLs in kidney of tamoxifen-inducible *Gpx4* KO mice 8 d after knockout induction. Notably, the same di- and tri-oxygenated PE species (PE-C18:0/C20:4 and PE-C18:0/C22:4) found in *Gpx4* KO cells were also present in the kidneys of *Gpx4* KO mice (**Fig. 4d,e**) and RSL-3-treated cells *in vitro* (**Fig. 5a,b**). This increase in di- and tri-oxygenated PE species was attenuated in mice treated with a ferroptosis inhibitor, liproxstatin-1 (**Fig. 4f**).

We constructed a Venn diagram (**Supplementary Fig. 5a**) to illustrate the commonality of four oxygenated PE species in the four ferroptotic conditions, including RSL3-treated WT and *Acsl4* KO cells, *Gpx4* KO cells (*in vitro*) and *Gpx4* KO mice (*in vivo*). The specificity of death signals was emphasized by the following two observations: (i) out of 62 PE species and 36 oxidizable PUFA-containing PE species, only 2 were identified as precursors of ferroptotic signals (**Supplementary Fig. 5b**), and (ii) out of 57 oxygenated PEs, only 4 were identified as specific ferroptotic signals (**Supplementary Fig. 5c**).

To further validate the identified oxygenated PE species as lipid death signals, we applied multivariate data analysis. Clear stratification of the data indicated the existence of potential biomarkers, thus enabling us to narrow down the phospholipid oxidation products with R2Y(cum) = 0.953, Q2(cum) = 0.908 (**Supplementary Fig. 5d**). All four oxygenated PEs were confirmed as biomarkers, with variable importance values for the projection (by orthogonal partial least-squares discriminant analysis) > 1 (**Supplementary Fig. 5e**).

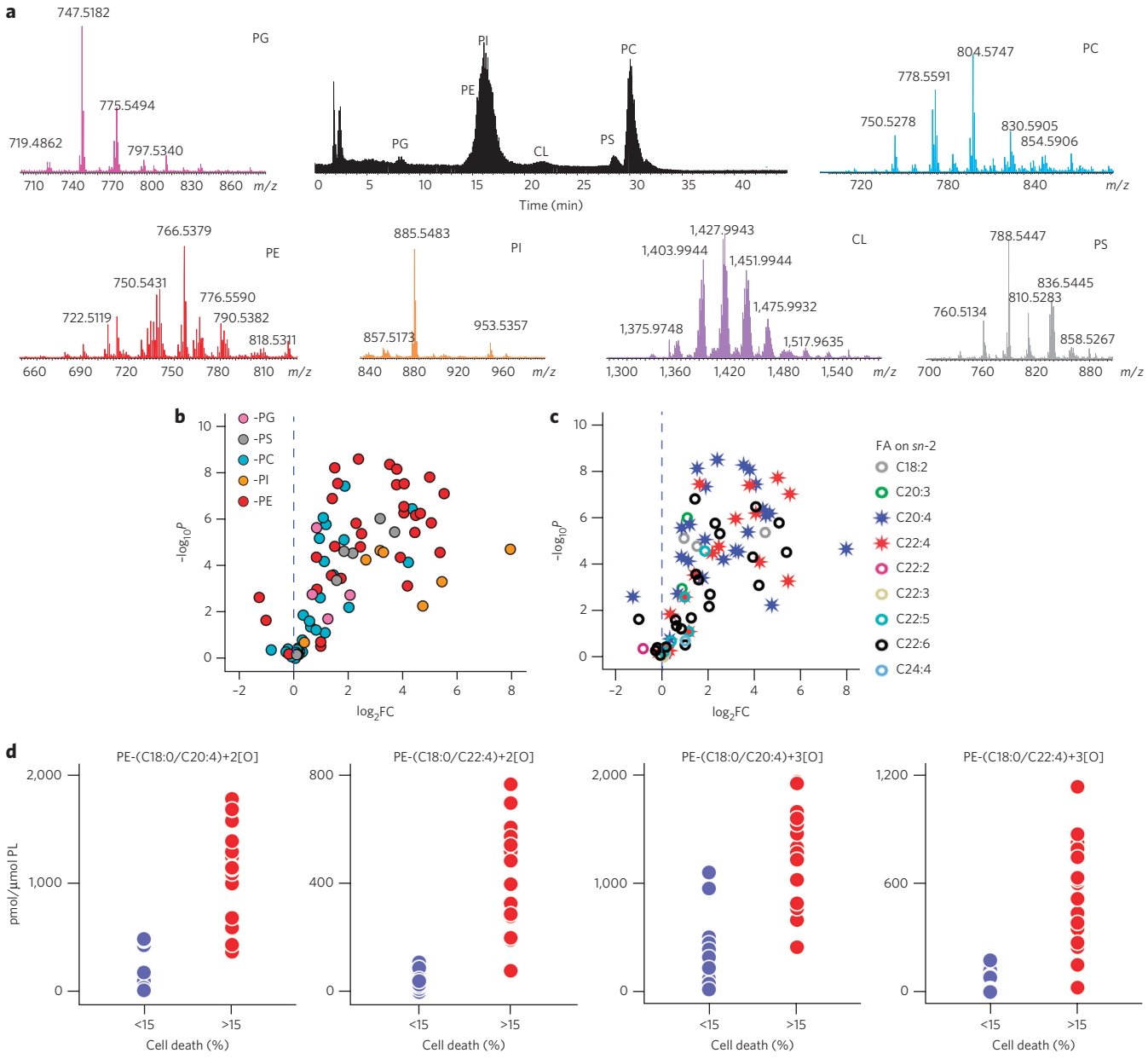

Figure 3 | Screening of phospholipids and their oxidation products identifies ferroptosis death signals. (**a**) Representative normal-phase LC-MS/MS chromatogram and mass spectra for six major classes of phospholipids in Pfa1 cells. (**b**) Scatter plot of RSL3-induced change in levels of oxygenated phospholipids in ferroptotic (cell death >15%, number of replicate data points = 18) versus live (cell death <15%, number of replicate data points = 26) cells. No oxygenated CLs were found. FC, fold change. (**c**) Scatter plot of RSL3-induced changes in oxygenated phospholipids after recategorization on the basis of fatty acyls (FA) in *sn*-2 positions. (**d**) Levels of di- and tri-oxygenated PE-(C18:0/C20:4) and PE-(C18:0/C22:4) in live (cell death <15%) and ferroptotic (cell death >15%) Pfa1 cells. Results from at least biological triplicates are presented unless otherwise specified.

LC-MS/MS identification of ferroptotic signals

By employing stable-isotopic labeling with deuterated AA (AA-d8), we established that AA-d8 can be elongated into AdA-d8, which was detectable as free fatty acid along with AA-d8-CoA, AdA-d8-CoA (**Supplementary Fig. 6**) and a variety of relatively abundant AA-d8- and AdA-d8-containing phospholipids (**Fig. 5c**). Significant accumulation of di- and tri-oxygenated diacyl-PE species containing C18:0/C20:4-d8 and C18:0/C22:4-d8 in the *sn*-2 position was detected in RSL3-triggered cells (**Fig. 5a**,**b**). No changes in the abundance of alkyl or alkenyl PE species were found (**Fig. 5d**). Accumulation of nondeuterated and deuterated PE was more robust in WT cells than in *Ascl4* KO cells (**Fig. 5c** and **Supplementary Fig. 7**).

Addition of RSL3 to cells supplemented with AA-d8 resulted in the formation of 20 deuterated oxygenated phospholipid species (110 of the total 130 remained nondeuterated). Among these we found accumulation of mono-, di- and tri-oxygenated species of diacyl-PE (**Fig. 5a**,**b**). MS/MS analysis confirmed the presence of oxidatively modified AA (**Fig. 5e**) and AdA (**Supplementary Fig. 8a**) in PE. These species were similar to those formed in nonsupplemented cells (**Fig. 5a**,**b**), and their content was lower in *Acsl4* KO cells than in WT cells. Tri-oxygenated deuterated PE products were not detectable in *Acsl4* KO cells (**Fig. 5a**,**b**). A small degree of accumulation of AA-d8 was detected in PC and was not affected by *Acsl4* KO (**Supplementary Fig. 8b**). Thus,

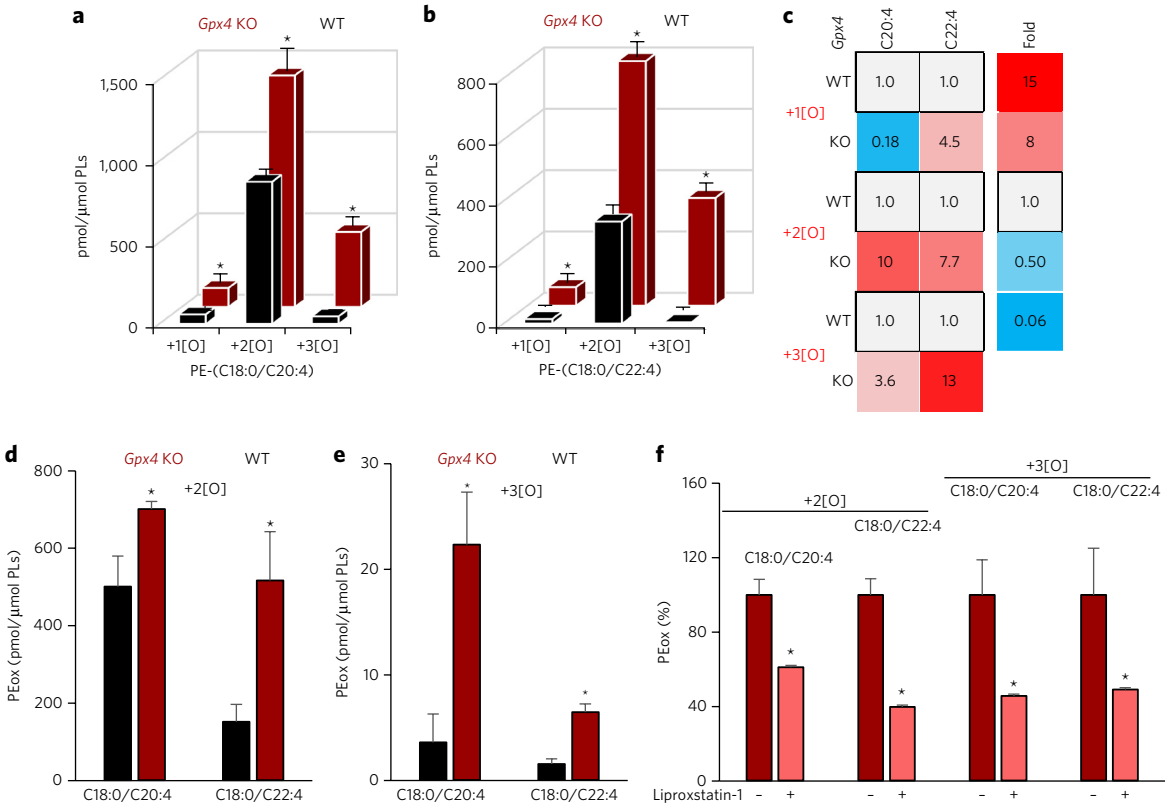

Figure 4 | Oxygenated PE species identified in ferroptotic *Gpx4* KO cells and kidney of *Gpx4* KO mice. (**a**) Accumulation of oxygenated PE-(C18:0/C20:4) (**a**) or PE-(C18:0/C22:4) (**b**) in WT and *Gpx4* KO cells. Data are mean ± s.d., $n = 3$. *$P < 0.05$ versus WT Pfa1 cells (*t*-test). (**c**) LC-MS-based heat map showing fold changes in oxygenated esterified C20:4 and C22:4 in WT and *Gpx4* KO Pfa1 cells. (**d**,**e**) Levels of di-oxygenated (**d**) and tri-oxygenated (**e**) species of PE-(C18:0/C20:4) and PE-(C18:0/C22:4) (PEox) in kidney of *Gpx4* KO mice. Data are mean ± s.d., $n = 3$. *$P < 0.05$ versus WT (*t*-test). (**f**) The ferroptosis inhibitor liproxstatin-1 decreases the accumulation of di- and tri-oxygenated PE species in kidney of GPX4-deficient mice. Data are mean ± s.d., $n = 3$. *$P < 0.05$ versus mice without liprostatin-1 (*t*-test). Results from at least biological triplicates are presented unless otherwise specified.

oxidation of AA- and AdA-containing PE represents the major pathway for ferroptotic signaling.

PE ferroptotic precursors are decreased in *Acs4* KO cells.

AA or AdA esterification into PE can be pharmacologically suppressed by rosiglitazone[13,19]. Lipidomics of WT Pfa1 cells treated with rosiglitazone (30 µM for 72 h) indicated reduced levels of PE molecular species with C18 fatty acids (C18:0 or C18:1) at the *sn*-1 position and C20:4 or C22:4 fatty acids at the *sn*-2 position, the latter of which are oxidation substrates for ferroptotic signals (**Supplementary Fig. 9a**). We observed a similar effect in *Acsl4* KO cells (**Supplementary Fig. 9b**). Rosiglitazone does not cause these changes in *Acsl4* KO cells[13,19]. The rosiglitazone effects were specific to C18 PE species at the *sn*-1 position, as no differences in the contents of PE with C16 fatty acids at the *sn*-1 position—which are not oxidized to proferroptotic death signals—were observed (**Supplementary Fig. 9**). Principal component analysis showed that rosiglitazone and ACSL4 deficiency caused similar changes in PE profiles[13]. Clustering analysis demonstrated that PE profiles in WT cells exposed to rosiglitazone were similar to those found in both untreated and rosiglitazone-treated *Ascl4* KO cells[13].

Direct oxygenation of PE generates ferroptotic signals

There are two alternative pathways for PE oxygenation during ferroptosis: (i) nonoxygenated AA or AdA (or their acyl-CoA-forms) is esterified into PE, which is then oxygenated, or (ii) free AA or AdA (or their acyl-CoA-forms) is oxygenated then esterified into PE. Accordingly, resistance of *Acsl4* KO cells to ferroptosis induction may be due either to lower levels of AA-PE and AdA-PE undergoing subsequent oxygenation or to lower integration of oxygenated AA or AdA into PE. We found that 15-LOX readily oxidizes AA-CoA, yielding AA-OOH-CoA with characteristic LC-MS fragmentation profiles (**Supplementary Fig. 10**). However, biosynthetically preformed AA-OOH-CoAs did not stimulate RSL3-induced ferroptosis (beyond the stimulatory effect of AA or AA-OOH) in WT or *Acsl4* KO cells (**Fig. 6a**). Moreover, no oxygenated AA-CoA or AdA-CoA was detected in WT or *Acsl4* KO cells challenged with RSL3, and oxygenated AA-PE and AdA-PE accumulated during RSL3-triggered ferroptosis in WT cells (**Fig. 5a**,**b**). Finally, exogenously preformed PE-AA-OOH—but not AA-OOH—strongly enhanced RSL3-triggered ferroptosis in *Acsl4* KO cells, thus directly demonstrating the role of PE-OOH as a ferroptotic death signal overriding the insufficiency of AA esterification into PE (**Fig. 6b**). After supplementation, PE-OOH abundance in cells was ~6 nmol/µmol phospholipids, which is comparable to that in AA-treated WT cells exposed to RSL3.

To authenticate the oxygenated PE species, we oxidized PE-(C18:0/C20:4) by human 15-LOX in the presence of lysates from control (untreated) and RSL3-treated (for 6 h) cells and established by LC-MS/MS (**Supplementary Fig. 11a**) that the enzymatic products were identical to the PE species with single-, double- and triple-oxygenated AA detected in ferroptotic cells (**Fig. 5e**). Levels of double-oxygenated hydroperoxy-PE species (PE-OOH) were higher in the presence of RSL3-treated cell lysates (versus control cell lysates) (**Supplementary Fig. 12**). Further, we incubated purified PE-OOH (prepared by preoxidation of PE-(C18:0/C20:4) by 15-LOX) with cell lysates and performed MS/MS analysis. We confirmed the structure of single- and double-oxygenated

PE as 15-hydroxy-AA-PE (**Supplementary Fig. 11c**) and 15-hydroperoxy-AA-PE species (**Fig. 6c**). The MS^2 and MS^3 analysis revealed that tri-oxygenated PE species were represented by 15-hydroperoxy-8-hydroxy-AA-PE, 15-hydroperoxy-9-hydroxy-AA-PE and 15-hydroperoxy-12-hydroxy-AA-PE (**Fig. 6c**). Moreover, we observed that addition of 15-LOX to lysates from RSL3-treated Pfa1 wild-type cells generated more PE-(C18:0/C20:4+3[O]) and less PE-(C18:0/C20:4+1[O]) than untreated cells (**Supplementary Fig. 12**). Similar results were obtained in *Gpx4* KO cell lysates (**Supplementary Fig. 11b**).

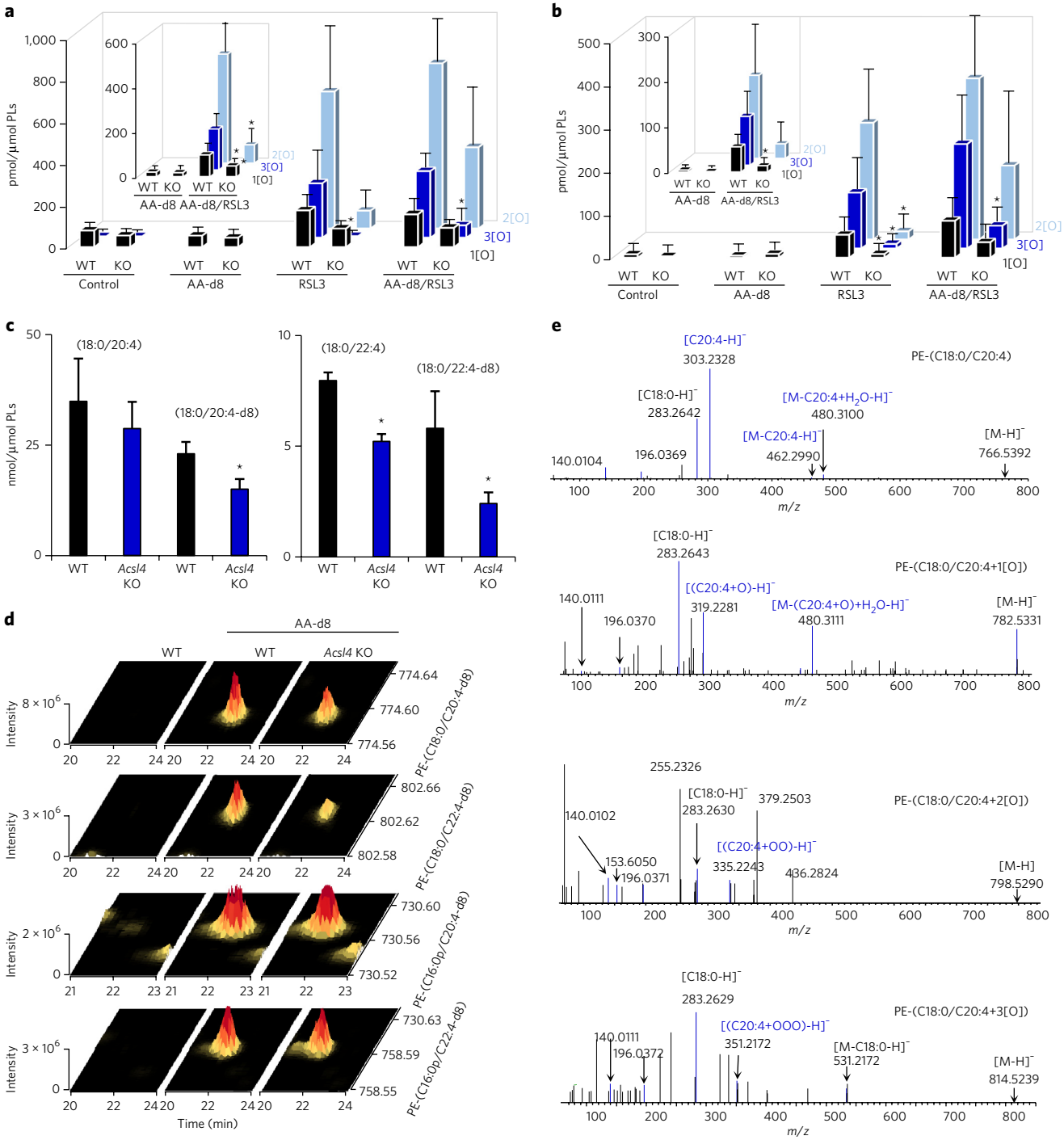

Figure 5 | Labeling with AA-d8 unravels pathways leading to oxygenated diacylated PE ferroptotic signals. (**a**,**b**) Accumulation of nondeuterated (main) and deuterated (inset) oxygenated PE-(18:0/20:4) (**a**) or PE-(18:0/22:4) (**b**) in WT and *Acsl4* KO cells treated with AA-d8 only (16 h) or AA-d8 (16 h) followed by RSL3 (AA-d8/RSL3) (100 nM, 6 h). Control, untreated cells. Data are mean ± s.d., $n = 3$. $^*P < 0.05$ versus WT Pfa1 cells (*t*-test). (**c**) Quantitative assessment of PE molecular species (C18:0/C20:4 and C18:0/C20:4-d8) (left) and (C18:0/22:4 and C18:0/C22:4-d8) (right) in WT and *Acsl4* KO Pfa1 cells treated with AA-d8. Data are mean ± s.d., $n = 3$. $^*P < 0.05$ versus WT (*t*-test). (**d**) 3D representation of mass spectra of deuterated PE from WT and *Acsl4* KO cells treated with AA-d8. p, plasmalogen. (**e**) Typical MS/MS spectrum illustrating fragmentation of nonoxygenated PE-(C18:0/C20:4) species as well as mono-, di- and tri-oxygenated species formed in RSL3-treated Pfa1 cells. Results from at least biological triplicates are presented unless otherwise specified.

Enzymatic generators of peroxidation signals

Several enzymes—such as LOX, cyclooxygenase (COX) and cytochrome P450 (CYP450)—can oxygenate AA and AdA. Among several specific regulators, inhibitors of LOX but not COX or CYP450 were effective in preventing ferroptotic death (**Fig. 6d**). Accordingly, liproxstatin-1 inhibited the 15-LOX enzymatic activity

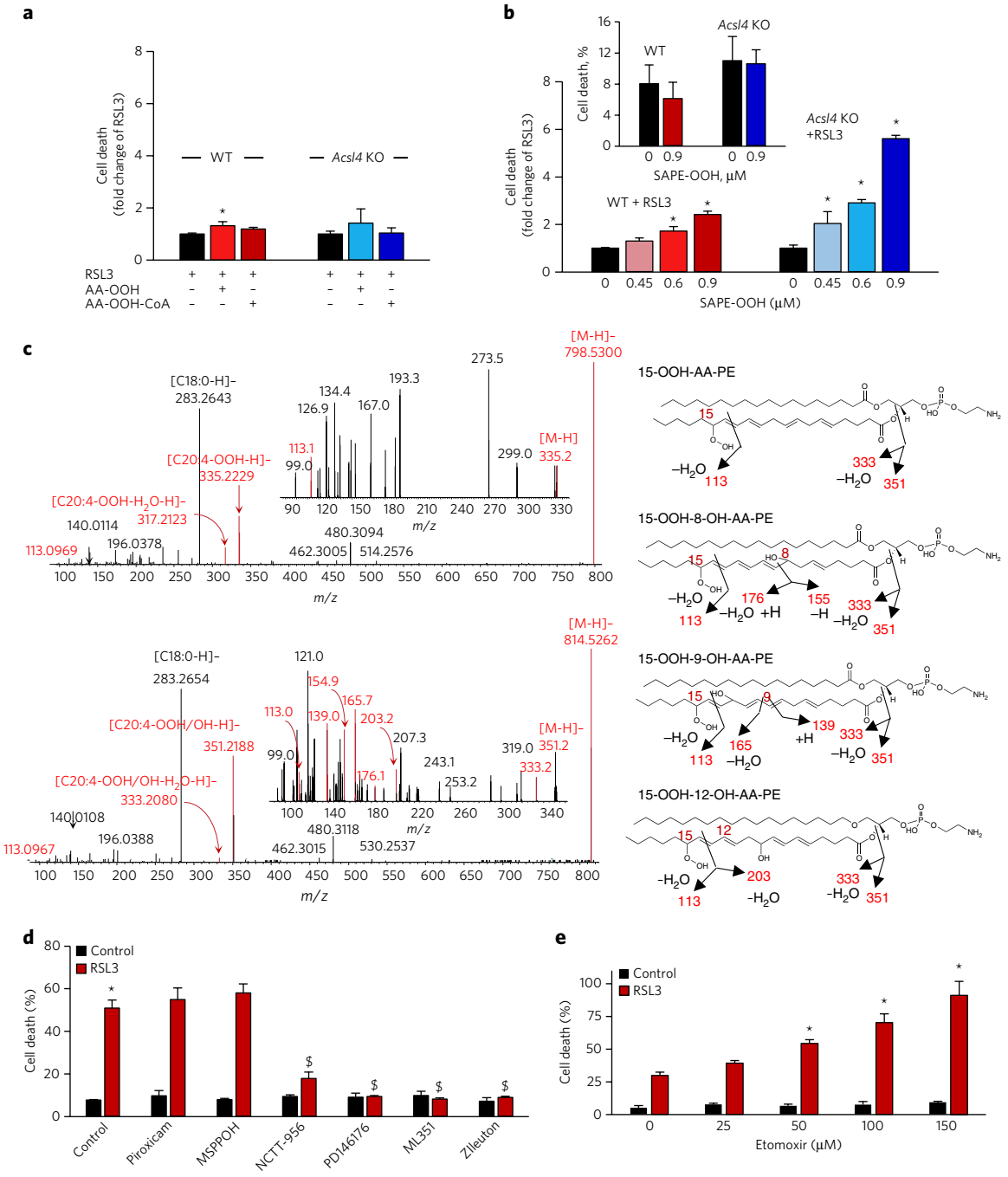

Figure 6 | A 15-LOX phospholipid oxidation product, 15-hydroperoxy-SAPE, triggers ferroptosis in WT and *Acsl4* KO Pfa1 cells. (**a**,**b**) Effects of AA-OOH (2.5 μM) and AA-OOH-CoA (2.5 μM) (**a**) and SAPE-OOH (**b**) on RSL3-triggered ferroptosis in WT or *Acsl4* KO cells. Inset (**b**) shows data for cells not treated with RSL3. RSL3 was used at 100 nM, and cells were treated for 6 h. Lactate dehydrogenase release levels: 8.1% (WT), 6.2% (WT + SAPE-OOH), 11% (*Acsl4* KO), 10.6% (*Acsl4* KO + SAPE-OOH). Data are mean ± s.d., $n = 3$; $^*P < 0.05$ (*t*-test). (**c**) LC-MS identification of 15-LOX-induced SAPE oxidation products in cell lysates. Left, MS^2 (main) and MS^3 (inset) fragmentation of di-oxygenated (top) and tri-oxygenated (bottom) SAPE. Right, structures of oxygenated SAPE and detected fragments (red). Identified products were 15-OOH-AA-PE, 15-OOH-8-OH-AA-PE, 15-OOH-9-OH-AA-PE and 15-OOH-12-OH-AA-PE. Characteristic fragments formed: *m/z* 351 and *m/z* 333, carboxylate anions of AA-OOH and AA-OOH minus H_2O, respectively; *m/z* 113, OOH at fifteenth carbon of AA; *m/z* 176 and 155, 165 and 139 and 203, OH at the eighth, ninth and twelfth carbons of AA. (**d**) RSL3-induced (50 nM, 18 h) ferroptosis in WT cells treated with inhibitors of LOX (ML351 (10 μM), PD146176 (0.5 μM), zileuton (10 μM) and NCTT (20 μM)), COX (piroxicam (20 μM)) or P450 (MSPPOH (10 μM)). Control, untreated cells. Data are mean ± s.d., $n = 3$. $^*P < 0.05$ versus control; $^{\$}P < 0.05$ versus RSL3 (*t*-test). (**e**) Etomoxir (β-oxidation inhibitor) enhances RSL3-induced (100 nM, 6 h) ferroptosis in WT cells. Data are mean ± s.d., $n = 3$. $^*P < 0.05$ versus RSL3 without etomoxir (*t*-test). Results from at least biological triplicates are presented unless otherwise specified.

(**Supplementary Fig. 13**) and suppressed the production of proferroptotic oxygenated PE *in vivo* (**Fig. 4f**). Computational modeling showed that liproxstatin-1 binds with 15-LOX with high affinity (binding energy −8.1 ± 0.2 kcal/mol). In contrast, COX cannot effectively utilize esterified PUFA as a substrate[20]. Some isoforms of CYP450 (such as P450 2W1) oxidize free fatty acids at low rates and catalyze oxidation (epoxidation, hydroxylation) of *sn*-1 PUFA lysophospholipids[21]. Notably, diacyl-glycerophospholipids are not used by CYP450 as oxygenation substrates. We further established that etomoxir, an inhibitor of PUFA β-oxidation, did not suppress but rather stimulated RSL3-induced cell death (**Fig. 6e**). This suggests that preservation of PUFA for enzymatic oxygenation reactions is conducive to the production of cell death signals.

Vitamin E regulates ferroptosis via LOX suppression

The vitamin E family comprises several homologs of tocopherols and tocotrienols known to effectively inhibit LOXes[22]. Both tocopherols and tocotrienols protected against ferroptotic death in *Gpx4* KO cells (**Supplementary Fig. 14a**), but tocotrienols were overall markedly more effective than tocopherols, which is in line with their higher effectiveness as inhibitors of LOX PUFA oxygenation. Tocopherols strongly suppress nonregiospecific free radical component of LOX-catalyzed peroxidation of phospholipids[23], but they can also act via competition for PUFA substrate binding sites (via the 'corking' mechanism). Computational modeling showed that LOX binds with different members of the vitamin E family but has a higher affinity for tocotrienols than for tocopherols (**Supplementary Fig. 14b**). If the competitive binding of tocopherols contributes to the suppression of LOX activity, then esterified derivatives of tocopherols should also exert this effect, in spite of the lack of radical-scavenging chromanol hydroxy group. Using electron spin resonance (ESR) spectroscopy, we confirmed that 15-LOX was ineffective in generating tocopheroxyl radicals, 1-electron oxidation intermediates from α-tocopherol succinate (TS) or α-tocopherol phosphate (TP), which were readily detectable as partially resolved characteristic signals from either α-tocopherol or α-tocotrienol (**Supplementary Fig. 14c**). However, both esterified analogs acted as 15-LOX inhibitors, but TS was markedly more efficient that TP (**Supplementary Fig. 14d**). Suppression of 15-LOX activity by TS was quantitatively comparable to that by α-tocotrienol. We performed LC-MS assessments of changes in the contents of α-tocopherol, TP, TS and α-tocotrienol after incubation with 15-LOX and AA. The levels of TS and TP were only slightly affected by the enzyme (**Supplementary Fig. 14e**). Thus, radical scavenging can contribute to the inhibitory effects of α-tocopherol and α-tocotrienol along with their ability to compete for the substrate binding site (**Supplementary Fig. 14**). For TS and TP, the corking mechanism may be the major contributor to inhibition of the activity. In line with this, computational modeling demonstrated that TS and TP interact with the protein in the tail-in orientation (**Supplementary Fig. 14b**).

LOX oxidizes nonbilayer phospholipid arrangements

Phospholipase A_2 (PLA_2) hydrolysis controls the availability of free PUFA to initiate the conventional LOX biosynthesis of lipid mediators[24]. How is AA esterified into phospholipids recognized by LOX? Our computational modeling demonstrated the feasibility of oxygenation of AA esterified into PE by 15-LOX; the binding energies were similar for free and esterified PUFA (**Supplementary Fig. 15a**). How the enzyme chooses its substrates from numerous AA-containing phospholipids is still unknown. One possible mechanism may be preferential attack of nonbilayer arrangements of phospholipid substrates, providing easier access for LOX (PE typically forms nonbilayer arrangements in the membrane)[25]. To test this possibility, we used stearoyl-AA-PE (SAPE), which forms nonbilayer (hexagonal) phases[26], and compared its oxidation with stearoyl-AA-PC (SAPC) with the typical bilayer organization (**Supplementary Fig. 15b**). SAPE was a much better 15-LOX substrate than SAPC (**Supplementary Fig. 15b**). AA-OOH-PE species were detected as the major oxidation products. These results are supported by coarse-grained molecular dynamics simulations demonstrating that 15-LOX binds robustly with SAPE but not with SAPC (**Supplementary Fig. 15c** and **Supplementary Table 2**).

Modeling of the ferroptotic phospholipid metabolome

We constructed a mathematical model (47 differential equations) for the production of oxygenated PE species based on a simplified network of main metabolic reactions regulating ferroptosis and focused on ferroptotic responses driven by GPX4 and AA- or AdA-PE (**Supplementary Fig. 16a** and **Supplementary Tables 3–5**). The model quantitatively reproduced not only the data set for the model calibration (**Supplementary Fig. 16b–e**) but also the additional data set reserved for model validation (**Supplementary Fig. 16f,g**). This indicates that the network covers key ferroptotic regulators and, possibly, the effects of other mechanisms that are not included in the model but are implicitly captured by its parameters (**Supplementary Figs. 16h–j** and **17a,b**).

DISCUSSION

The term ferroptosis was coined to describe one of the programmed death pathways associated with the dysregulation of thiol and lipid oxidative metabolism controlled by GPX4. GPX4 deficiency leads to the accumulation of reactive lipid electrophiles[27]. Given the unique ability of GPX4 to catalyze the reduction of PL-OOH, their accumulation is highly likely in the context of GPX4 deficiency. In spite of the commonly suggested role of phospholipid peroxidation products in ferroptosis, the proximate phospholipid peroxidation products have not been identified. Here we identified four molecular species of doubly and triply oxygenated diacyl AA- or AdA-containing species of PE containing 15-hydroperoxy groups as ferroptotic death signals. Oxygenation attack occurs on AA- and AdA-PE but not via re-esterification of preoxidized free fatty acids into phospholipids. Exogenous AA- and AdA-PE-OOH—but not free AA-OOH or AdA-OOH—caused ferroptotic cell death. Mono-oxygenated PE products—formed by esterification of enzymatically presynthesized free eicosanoids—have been implicated in signaling functions of innate immune cells[20]. These products, however, were formed by fast esterification of enzymatically presynthesized free eicosanoids, and the relevant reactions were localized predominantly to the nuclear and extranuclear membrane. Direct oxygenation of PUFA-PE species by 12/15-LOX has been documented in plasma membranes of resident macrophages as a required mechanism for the uptake and phagocytosis of apoptotic cells[28].

Oxidation of CLs—a required step in the execution of apoptosis[29]—was not involved in ferroptotic signaling. Thus redox signaling in apoptosis and ferroptosis is based on specific engagement of two different classes of phospholipids, CL and PE, with different acyl molecular speciation—linoleic acid (C18:2) oxygenation in CLs and AA or AdA oxygenations of PE. The oxygenating enzymes are also different—cytochrome c (ref. 30) and probably 15-LOX, respectively. Live cell imaging demonstrated predominant accumulation of PE-OOH in the extramitochondrial ER-associated compartments, where COX, LOX and CYP450 can generate PUFA lipid hydroperoxides[31]. Of those, only LOXes, however, utilize diacyl lipids as their substrates[32], thus making these enzymes possible candidates for catalysts of ferroptotic oxygenated PE species. Our model biochemical experiments and computer simulations indicate that nonbilayer (possibly hexagonal) arrangements of AA- and AdA-PE, in contrast to the highly ordered bilayer organization of AA-PC, facilitate the availability of these phospholipid substrates for binding and enzymatic attack by 15-LOX. It is also possible that the prevalence of PE in the inner leaflet of plasma membrane[33,34] contributes to the preferential oxidation by

LOX, whereas confinement of PC to the outer membrane monolayer is not conducive to its interactions with the intracellular oxidizing machinery.

A highly organized oxygenation center in the ER-associated compartment may be functionally involved in the production of eicosanoids and docosanoids under redox control of GPX4 over metabolic reaction of PUFA-OOH. Insufficiency of this control caused by genetic or chemical inactivators leads to accumulation of excessive amounts of highly electrophilic and diffusible lipid mediators, threatening the viability of many surrounding cells. Insufficiency of GPX4 triggers lipid metabolic pathways for the enhanced production of AA- or AdA-containing diacylated PEs as substrates of LOX-catalyzed reactions. This leads to the generation of doubly and triply oxygenated 15-hydroperoxy-containing PE species acting as lipid death signals. The significance of functional association of ACSL4, elongase 5, LPCAT3 and LOX for the production of PE-AA-OOH and PE-AdA-OOH was further emphasized by our systems biology analysis, which confirmed high sensitivity of several key enzymes (ACSL4, LPCAT3 and 15-LOX) for ferroptosis. Notably, the presence of LOXes has been discovered in *Pseudomonas aeruginosa*, prokaryotes that lack polyunsaturated lipid substrates[35]. It appears that the bacteria utilize secretable LOX to cause ferroptotic death of target epithelial cells. This suggests that LOX-driven selective oxidation of esterified PE may represent a highly conserved and ancient mechanism of cell death.

The essentiality of esterified oxygenated PUFA explains the recently demonstrated importance of ACSL4 and LPCAT3 as participants in ferroptotic lipid signaling, thus offering new pharmacological targets for drug discovery[13,16]. Moreover, different forms of vitamin E, particularly tocotrienols, are effective in protecting against ferroptotic death. Thus, one of the physiologically possible mechanisms of vitamin E action may be specific liganding of the LOX catalytic site outcompeting binding and oxygenation of free or PE-esterified AA and AdA. Our computational modeling of free PUFAs, including AA and AdA, shows that the tail-in orientation is the dominant alignment of the substrate in the catalytic site. Previous studies using a quantum mechanics–molecular mechanics approach[36] have shown that hydrogen abstraction from C_{13} by 15-LOX-2 is consistent only with the tail-in orientation of AA, and its carboxylate group interacts with Arg429, located at the opening of the substrate binding site.

It has been reported that 15-LOX generates not only regiospecific (phospho)lipid hydroperoxides but also random hydroperoxides as side reaction products[37]. Radical-scavenging antioxidants (α-tocopherol and 2-carboxy-2,5,7,8-tetramethyl-6-chromanol) were more effective in inhibiting the formation of random oxidation products rather than regiospecific products. Thus, not only free radical scavenging but also competition with the oxidation substrates for the binding site of the protein (corking mechanism) may be an important factor in the inhibition of stereo-specific LOX-driven oxidations. Several reports have documented the efficiency of vitamin E as a protector of cells against ferroptotic death *in vitro*[38–40]. In a previous publication[18], we reported that α-tocopherol was effective in preventing ferroptosis at nanomolar concentrations. More importantly, this protective effect of vitamin E was also realized *in vivo*[41]. It has been established that *Gpx4*$^{-/-}$ pups born from mothers fed a vitamin-E-enriched diet survived, yet this protection was reversible, as subsequent vitamin E deprivation caused death of GPX4-deficient mice ~4 weeks thereafter[38]. Thus, vitamin E can be considered an effective antiferroptotic agent. Our data show that tocotrienols are even more effective in protecting cells against ferroptosis. This higher efficiency may be due to better integration of tocotrienols into cells[42] or to their competing more effectively with PUFA-PL substrates for binding sites on 15-LOX. As 15-LOX is an important contributor to proferroptotic PE peroxidation, substantial inhibitory activity of TP and TS toward 15-LOX, in the absence of radical scavenging hydroxy groups, points to an alternative mechanism of action, such as competition for the substrate binding site (i.e., corking).

Previous studies indicate that induction of ferroptotic death pathways can be used to eradicate cancer cells resistant to proapoptotic stimulation[43]. Given the stimulatory role of AA and AdA in inducing ferroptotic cell death, it is possible that nutritional approaches to treatment of cancer could be combined with ferroptotic inducers (such as RSL3 or other inducers or GSH depletion) to enhance anticancer therapy. In particular, the antitumor phenolic drug etoposide effectively removes GSH in myeloperoxidase-rich myelogenous leukemia cells, thus incapacitating GPX4 and triggering ferroptosis. It is tempting to speculate that mechanisms of several well-characterized regulators of ferroptosis—such as regulators of GSH synthesis and transport, the redox-sensitive Nrf2 signaling pathway and metabolic regulators of iron uptake and metabolism—converge on the specific oxygenation of PE as ferroptotic signals.

Received 3 March 2016; accepted 3 October 2016;
published online 14 November 2016

METHODS

Methods, including statements of data availability and any associated accession codes and references, are available in the online version of the paper.

References

1. Allocati, N., Masulli, M., Di Ilio, C. & De Laurenzi, V. Die for the community: an overview of programmed cell death in bacteria. *Cell Death Dis.* **6**, e1609 (2015).
2. Byrne, J.M. *et al.* Redox cycling of Fe(II) and Fe(III) in magnetite by Fe-metabolizing bacteria. *Science* **347**, 1473–1476 (2015).
3. Dixon, S.J. & Stockwell, B.R. The role of iron and reactive oxygen species in cell death. *Nat. Chem. Biol.* **10**, 9–17 (2014).
4. Dixon, S.J. *et al.* Ferroptosis: an iron-dependent form of nonapoptotic cell death. *Cell* **149**, 1060–1072 (2012).
5. Yang, W.S. & Stockwell, B.R. Ferroptosis: death by lipid peroxidation. *Trends Cell Biol.* **26**, 165–176 (2016).
6. Yang, W.S. & Stockwell, B.R. Synthetic lethal screening identifies compounds activating iron-dependent, nonapoptotic cell death in oncogenic-RAS-harboring cancer cells. *Chem. Biol.* **15**, 234–245 (2008).
7. Imai, H. & Nakagawa, Y. Biological significance of phospholipid hydroperoxide glutathione peroxidase (PHGPx, GPx4) in mammalian cells. *Free Radic. Biol. Med.* **34**, 145–169 (2003).
8. Yamanaka, K. *et al.* A novel fluorescent probe with high sensitivity and selective detection of lipid hydroperoxides in cells. *RSC Advances* **2**, 7894–7900 (2012).
9. Drummen, G.P., van Liebergen, L.C., Op den Kamp, J.A. & Post, J.A. C11-BODIPY$^{581/591}$, an oxidation-sensitive fluorescent lipid peroxidation probe: (micro)spectroscopic characterization and validation of methodology. *Free Radic. Biol. Med.* **33**, 473–490 (2002).
10. Li, B. & Pratt, D.A. Methods for determining the efficacy of radical-trapping antioxidants. *Free Radic. Biol. Med.* **82**, 187–202 (2015).
11. Küch, E.M. *et al.* Differentially localized acyl-CoA synthetase 4 isoenzymes mediate the metabolic channeling of fatty acids towards phosphatidylinositol. *Biochim. Biophys. Acta* **1841**, 227–239 (2014).
12. Golej, D.L. *et al.* Long-chain acyl-CoA synthetase 4 modulates prostaglandin E release from human arterial smooth muscle cells. *J. Lipid Res.* **52**, 782–793 (2011).
13. Doll, S. *et al.* ACSL4 dictates ferroptosis sensitivity by shaping cellular lipid composition. *Nat. Chem. Biol.* http://dx.doi.org/10.1038/nchembio.2239 (2016).
14. McIntyre, T.M., Prescott, S.M. & Stafforini, D.M. The emerging roles of PAF acetylhydrolase. *J. Lipid Res.* **50** (Suppl.): S255–S259 (2009).
15. Soh, N. *et al.* Swallow-tailed perylene derivative: a new tool for fluorescent imaging of lipid hydroperoxides. *Org. Biomol. Chem.* **5**, 3762–3768 (2007).
16. Dixon, S.J. *et al.* Human haploid cell genetics reveals roles for lipid metabolism genes in nonapoptotic cell death. *ACS Chem. Biol.* **10**, 1604–1609 (2015).
17. Seiler, A. *et al.* Glutathione peroxidase 4 senses and translates oxidative stress into 12/15-lipoxygenase dependent- and AIF-mediated cell death. *Cell Metab.* **8**, 237–248 (2008).
18. Friedmann Angeli, J.P. *et al.* Inactivation of the ferroptosis regulator Gpx4 triggers acute renal failure in mice. *Nat. Cell Biol.* **16**, 1180–1191 (2014).

19. Askari, B. *et al.* Rosiglitazone inhibits acyl-CoA synthetase activity and fatty acid partitioning to diacylglycerol and triacylglycerol via a peroxisome proliferator-activated receptor-γ-independent mechanism in human arterial smooth muscle cells and macrophages. *Diabetes* **56**, 1143–1152 (2007).
20. O'Donnell, V.B. & Murphy, R.C. New families of bioactive oxidized phospholipids generated by immune cells: identification and signaling actions. *Blood* **120**, 1985–1992 (2012).
21. Xiao, Y. & Guengerich, F.P. Metabolomic analysis and identification of a role for the orphan human cytochrome P450 2W1 in selective oxidation of lysophospholipids. *J. Lipid Res.* **53**, 1610–1617 (2012).
22. Khanna, S. *et al.* Molecular basis of vitamin E action: tocotrienol modulates 12-lipoxygenase, a key mediator of glutamate-induced neurodegeneration. *J. Biol. Chem.* **278**, 43508–43515 (2003).
23. Arai, H., Nagao, A., Terao, J., Suzuki, T. & Takama, K. Effect of D-α-tocopherol analogues on lipoxygenase-dependent peroxidation of phospholipid–bile salt micelles. *Lipids* **30**, 135–140 (1995).
24. Dennis, E.A. Diversity of group types, regulation, and function of phospholipase A2. *J. Biol. Chem.* **269**, 13057–13060 (1994).
25. van den Brink-van der Laan, E., Killian, J.A. & de Kruijff, B. Nonbilayer lipids affect peripheral and integral membrane proteins via changes in the lateral pressure profile. *Biochim. Biophys. Acta* **1666**, 275–288 (2004).
26. Lee, A.G. How lipids affect the activities of integral membrane proteins. *Biochim. Biophys. Acta* **1666**, 62–87 (2004).
27. Toppo, S., Flohé, L., Ursini, F., Vanin, S. & Maiorino, M. Catalytic mechanisms and specificities of glutathione peroxidases: variations of a basic scheme. *Biochim. Biophys. Acta* **1790**, 1486–1500 (2009).
28. Uderhardt, S. *et al.* 12/15-lipoxygenase orchestrates the clearance of apoptotic cells and maintains immunologic tolerance. *Immunity* **36**, 834–846 (2012).
29. Orrenius, S. & Zhivotovsky, B. Cardiolipin oxidation sets cytochrome *c* free. *Nat. Chem. Biol.* **1**, 188–189 (2005).
30. Kagan, V.E. *et al.* Cytochrome *c* acts as a cardiolipin oxygenase required for release of proapoptotic factors. *Nat. Chem. Biol.* **1**, 223–232 (2005).
31. Massey, K.A. & Nicolaou, A. Lipidomics of polyunsaturated-fatty-acid-derived oxygenated metabolites. *Biochem. Soc. Trans.* **39**, 1240–1246 (2011).
32. Kuhn, H., Banthiya, S. & van Leyen, K. Mammalian lipoxygenases and their biological relevance. *Biochim. Biophys. Acta* **1851**, 308–330 (2015).
33. Schroeder, F. Regulation of aminophospholipid asymmetry in murine fibroblast plasma membranes by choline and ethanolamine analogues. *Biochim. Biophys. Acta* **599**, 254–270 (1980).
34. Sessions, A. & Horwitz, A.F. Myoblast aminophospholipid asymmetry differs from that of fibroblasts. *FEBS Lett.* **134**, 75–78 (1981).
35. Garreta, A. *et al.* Structure and interaction with phospholipids of a prokaryotic lipoxygenase from *Pseudomonas aeruginosa*. *FASEB J.* **27**, 4811–4821 (2013).
36. Suardíaz, R. *et al.* Understanding the mechanism of the hydrogen abstraction from arachidonic acid catalyzed by the human enzyme 15-lipoxygenase-2. A quantum mechanics/molecular mechanics free energy simulation. *J. Chem. Theory Comput.* **12**, 2079–2090 (2016).
37. Noguchi, N. *et al.* The specificity of lipoxygenase-catalyzed lipid peroxidation and the effects of radical-scavenging antioxidants. *Biol. Chem.* **383**, 619–626 (2002).
38. Carlson, B.A. *et al.* Glutathione peroxidase 4 and vitamin E cooperatively prevent hepatocellular degeneration. *Redox Biol.* **9**, 22–31 (2016).
39. Chen, L., Hambright, W.S., Na, R. & Ran, Q. Ablation of the ferroptosis inhibitor glutathione peroxidase 4 in neurons results in rapid motor neuron degeneration and paralysis. *J. Biol. Chem.* **290**, 28097–28106 (2015).
40. Matsushita, M. *et al.* T cell lipid peroxidation induces ferroptosis and prevents immunity to infection. *J. Exp. Med.* **212**, 555–568 (2015).
41. Wortmann, M. *et al.* Combined deficiency in glutathione peroxidase 4 and vitamin E causes multiorgan thrombus formation and early death in mice. *Circ. Res.* **113**, 408–417 (2013).
42. Sen, C.K., Khanna, S., Roy, S. & Packer, L. Molecular basis of vitamin E action. Tocotrienol potently inhibits glutamate-induced pp60$^{c\text{-}Src}$ kinase activation and death of HT4 neuronal cells. *J. Biol. Chem.* **275**, 13049–13055 (2000).
43. Yang, W.S. *et al.* Regulation of ferroptotic cancer cell death by GPX4. *Cell* **156**, 317–331 (2014).

Acknowledgments

We thank J. Ruzicka (Thermo Fisher Scientific) for help in obtaining MS^3 spectra of PE oxidation products using tribrid Fusion Lumos. Supported by the US National Institutes of Health (P01HL114453 to R.K.M., U19AI068021 to J.G., NS076511 to V.E.K., NS061817 to H.B., P41GM103712 to I.B. and ES020693 to Y.Y.T.), the Human Frontier Science Program (HFSP-RGP0013/2014), and the Deutsche Forschungsgemeinschaft (CO 291/2-3 and CO 291/5-1) to M.C.

Author contributions

V.E.K., M.C. and H.B. formulated the idea, designed the study and wrote the manuscript. G.M. and J.P.F.A. performed cell experiments. Y.Y.T. and F.Q. performed MS lipid analysis, interpreted data. C.S. and S.W. performed cell imaging experiments. T.A., V.A.T. and A.A.A. performed model systems experiments. D.M. and J.K.-S. performed computational modeling. B.L. and I.B. performed network analysis. S.D., H.H.D., J.J., V.B.R., A.A.K., B.P. and Q.Y. participated in cell or animal experiments. J.G., R.K.M. and B.R.S. participated in formulating the idea and writing the manuscript. All authors discussed the results and commented on the manuscript.

Competing financial interests

The authors declare no competing financial interests.

Additional information

Any supplementary information, chemical compound information and source data are available in the online version of the paper. Reprints and permissions information is available online at http://www.nature.com/reprints/index.html. Correspondence and requests for materials should be addressed to V.E.K., M.C. or H.B.

ONLINE METHODS

Materials. All the lipid standards, 1-stearoyl-2-arachidonoyl-PE (SAPE) and 1-stearoyl-2-arachidonoyl phosphatidylcholine (SAPC) were purchased from Avanti Polar Lipids. AquaBluer was obtained from MultiTarget Pharmaceuticals. The Cytotoxicity Detection Kit for measuring the released lactate dehydrogenase (LDH) was purchased from Promega. LiperFluo was purchased from Dojindo Molecular Technologies, Inc. Deuterated arachidonic acid (AA-d8), triacsin C, and AA-hydroperoxy-derivative (AA-OOH), platelet-activating factor-acetylhydrolase (PAF-AH), 15-LOX from *Glycine max* and recombinant human 15-LOX-2 were purchased from Cayman Chemical. 5-(methylamino)-2-(1-naphthalenyl)-4-oxazolecarbonitrile (ML351), 6,11-dihydro-[1]benzothiopyrano[4,3-b]indole (PD146176), 4-hydroxy-2-methyl-3-(pyrid-2-*yl*-carbamoyl)-2H-1,2-benzothiazine 1,1-dioxide (piroxicam), *N*-(methylsulfonyl)-2-(2-propynyloxy)-benzenehexanamide (MSPPOH), (±)-*N*-hydroxy-N-(1-benzo[b]thien-2-ylethyl)urea (zileuton) and N-[(8-hydroxy-5-nitro-7-quinolinyl)-2-thienylmethyl]-propanamide (NCTT-956) were purchased from Sigma-Aldrich. GPX4-specific antibody (ab125066) was purchased from Abcam. β-actin-specific antibody was from Sigma-Aldrich (A3854) and primary Lpcat3-specific antibody, MBOAT5 (D-19) goat polyclonal IgG (sc-161831) were from Santa Cruz Biotechnology Inc. Secondary anti-goat IgG (whole molecule)-peroxidase antibody was produced in rabbit (A5420-1mL) and purchased from Sigma-Aldrich. All other reagents were purchased from Sigma-Aldrich unless indicated.

***Gpx4* KO mice.** *In vivo* experiments with C57BL/6J female or male mice (8–10 weeks old, obtained from Charles River Laboratories) were performed in Helmholtz Zentrum, Institute of Developmental Genetics (Münich, Germany). Generation of mice with *loxP*-flanked ('floxed') *Gpx4* alleles (*Gpx4*$^{fl/fl}$ (Gpx4^{tm2Marc})), referred to as *Gpx4* KO) was performed as previously described[17]. For the pharmacological inhibitor experiments, *CreER*^{T2};*Gpx4*$^{fl/fl}$ mice were injected on days 1 and 3 with 0.5 mg 4-hydroxytamoxifen dissolved in Miglyol. On day 4, compound treatment was started (liproxstatin-1: 10 mg/kg) along with vehicle control (1% DMSO in PBS). Liproxstatin-1 and vehicle control were administered once daily by intraperitoneal (i.p.) injection. Vehicle is colorless and liproxstatin-1 is white or light brown and has indistinguishable odor, ensuring no detectable bias. Supplementation of drinking water was done in a blinded fashion and animal behavior was assessed daily. Animals included in the treatment study were randomly distributed between both sexes and weight, and were typically 8–10 weeks of age. The average weight between the groups was typically 22–24 g. For the treatment experiments, mice were allocated such that groups had similar numbers of females and males of the same age. Mice of similar weights were chosen for each sex in each group. The injections and collection of (terminal) animals were done in a blinded fashion. When animals showed terminal signs (significant weight loss; inability to walk, groom, and eat; slow or labored breathing) (significant weight loss; inability to walk, groom, and eat; slow or labored breathing), they were sacrificed according to European animal welfare law. The treatment experiment using the inducible *Gpx4* KO mice was approved by the Regierung von Oberbayern (Bavaria, Germany) and performed under the animal protocol number 55.2-1-54-2532-144-12. Kidney tissue from mice was obtained from Helmholtz Zentrum, Institute of Developmental Genetics.

Cell lines, conditions and treatments. Mouse embryonic fibroblasts (MEFs) were purchased from ATCC. Cells were STR profiled at ATCC. *Acsl4* KO cells were generated using CRISPR–Cas9 technology[13]. Cas9-expressing mouse embryonic fibroblasts (Pfa1 cells) were transfected with a plasmid expressing a gRNA targeting exon 1 of the *Acsl4* gene. *Gpx4* conditional KO cells were generated by Cre–*loxP* technology as described previously[17]. 4-hydroxytamoxifen (Tam) was used to initiate mutated-estrogen receptor (MER)-Cre-MER-mediated excision of floxed *Gpx4* alleles to result in *Gpx4* KO cells. Mouse lung epithelial (MLE) cells were purchased from ATCC. MLE cells were cultured in HITES medium (DMEM/F12, 1:1 mix, with 5 μg/ml insulin, 10 μg/ml transferin, 30 nM sodium selenite, 10 nM hydrocortisone, 10 nM β-estradiol, 10 mM HEPES and 2 mM L-glutamine) supplemented with 10% FBS, 100 U/ml penicillin and 100 μg/ml streptomycin. All cells were maintained in DMEM with 10% FBS, 100 U/ml penicillin and 100 μg/ml streptomycin. Cells were grown in incubators with controlled temperature of 37 °C, 5% CO_2 and 95% humidity. All cell lines used here were routinely tested in the laboratory for mycoplasma contamination and were negative.

WT and *Acsl4* KO cells were pretreated with either AA (2.5 μM), 15-hydroperoxy-AA (AA-OOH) (2.5 μM) or 15-hydroperoxy-arachidonoyl-CoA (AA-OOH-CoA) (2.5 μM) in complete medium for 16 h followed by RSL3 treatment. In most experiments, RSL3 treatments were performed at a concentration of 100 nM for 6 h. For MLE cells, RSL3 was used at 0.5 or 1.0 μM for 6 h. Cell viability was assessed by propidium iodide staining or LDH release unless stated otherwise.

Treatment with 15-hydroperoxy-AA-PE. WT and *Acsl4* KO cells were treated with RSL3 (100 nM) in complete medium for 2 h followed by SAPE-OOH (0.45, 0.6 or 0.9 μM) for another 4 h in the presence of RSL3 before cell-death analysis. Cells were harvested by trypsinization for further analysis.

Live cell imaging. Cells were seeded in 35-mm glass-bottomed tissue culture dishes (MatTek Corp.) before infection with an adenoviral vector expressing either mitochondrially targeted (mito-FAP) or ER-targeted (ER-FAP) fluorogen activating protein[44]. 48 h after transfection, cells were prestained with 10 μM LiperFluo for 30 min then treated with 100 nM RSL3. Before imaging, cells were loaded with 5 nM malachite green to reveal the mito-FAP-encoding transgene (thereby defining the mitochondria or ER compartments)[45]. All images were acquired using a Nikon Ti inverted microscope equipped with a 60× 1.49 NA oil optic, SpectraX diode-based light source (Lumencor), Chroma Technology Inc. filer sets, and an ORCA-Flash4.0 V2 digital cMOS camera (Hamamatsu Photonics, K.K.). Images were acquired and analyzed using NIS-Elements software (Nikon Inc.).

Assessment of GPX4 activity. Activity measurements in cell lysates were performed in 0.1 M Tris-HCl (pH 8.0), containing 0.5 mM EDTA and 1.25% Triton X-100, 0.2 mM NADPH, 3 mM GSH, glutathione reductase (1 U/ml) and 0.5 mg cell protein. Oxidized tetralinoleoyl cardiolipin (final concentration 50 μM) was used as a substrate. The amount of oxidized GSH was calculated on the basis of the amount of NADPH consumed during the reduction of oxidized GSH (molar extinction coefficient of NADPH at 340 nm is 6.2×10^3 $mol^{-1}cm^{-1}$).

Western blot analysis of GPX4. Western blotting analysis was used to determine the abundance of GPX4 in the MEF cells. An equal amount of proteins was loaded in each lane. Proteins were separated on 8–16% gradient Tris-glycine gels (Precise 8–16% Tris-Glycine Gels, 25 μl/well, 15 wells) (Life Technologies) and electrically transferred to a PVDF membrane (Bio-Rad). After blocking the membrane with 5% skim milk, target proteins were immunodetected with GPX4-specific antibody at 1:500 (ab125066, Abcam) after overnight incubation at 4 °C. Thereafter, the horseradish peroxidase (HRP)-conjugated anti-rabbit IgG H&L (1:2,000, ab6721, Abcam) was applied as the secondary antibody, and bands were detected using Amersham ECL and western blotting detection reagents (GE Healthcare).

***Lpcat3* knockdown.** For the generation of *Lpcat3* KD in MLE or MEF cells, we used pSico plasmid (Addgene 11578), a lentivirus based Cre-*lox*-regulated RNA interference system. Briefly, small hairpin RNA (shRNA) oligos (sense, 5′ TGGCTTAAGGTGTACAGATCTTCAAGAGAGATCTGTACACTTTAA GCCTTTTTTC 3′; antisense, 5′TCGAGAAAAAAGGCTTAAGGTGTA CAGATCTCTCTTGAA GATCTGTACACCTTAAGCCA 3′) (Integrated DNA Technologies) were annealed by heating in annealing buffer for 4 min at 95 °C and then cooled to room temperature. Annealed oligos were ligated to pSico vector at HpaI and XhoI sites (Takara Bio USA, Inc.) with T4-DNA ligase enzyme (Promega). DNA was isolated from the positive clone from *E. coli* DH5α (Invitrogen) and transfected into MLE or MEF cells using Lipofectamine 3000 (Invitrogen). Transfected cells were sorted (three times) by selecting only GFP-positive cells by flow cytometry (BD FACSAria II). After the third sorting, more than 90% of cells were stable GFP-positive cells. To these cells, TAT-Cre recombinase (Excellgen) protein (1 μM) was added and the efficiency of *Lpcat3* KD was determined after 48, 72, and 96 h for MLE cells or 72 h for MEF cells by western blotting using anti-LPCAT3 (Sc-161831, Santa Cruz Biotechnology Inc.).

Western blot analysis of LPCAT3. Cells were harvested by trypsinization, washed with PBS, re-suspended in phosphate buffer (pH 7.8) and sonicated on ice. Protein concentrations were determined with a Bradford protein assay kit (Thermo Fisher Scientific). Equal amounts of protein were separated by 10% SDS–PAGE, electrotransferred by semidry blotting onto a nitrocellulose membrane and probed with primary antibodies to LPCAT3 at 1:1,000 dilution. Immunoreactive bands were detected by a chemiluminescence kit Thermo Fisher Scientific. The bands were visualized using X-ray film and imaged with computerized digital imaging system. (ImageJ). Actin antibody was used as a loading control.

Preparation of hydroperoxy PE. 1-steraoyl-2-arachidonoyl-PE was oxidized by 15-LOX from *Glycine max* in 25 mM borate buffer, pH 9, in the presence of 200 μM DTPA, 0.05% sodium cholate, 5 μM H_2O_2 at RT for 45 min. The incubation mixture was continuously bubbled with 95% O_2. At the end of incubation, PE-OOH was extracted and purified by HPLC (Shimadzu Corp.) using 4.4 × 150 mm 5 μm C18 column (Phenomenex). Isocratic mobile phase consists of acetonitrile/water/triethylamine/acetic acid (900:100:5:5, v/v) was used for separation. Purity was confirmed by LC/MS using LQX ion trap mass spectrometer (Thermo Fisher Scientific). Purified PE-OOH (99%) was reconstituted in DMSO and added to cells.

Identification of PE oxygenated products in cell lysates. WT Pfal1 cells were treated with RSL3 (100 nM) for 6 h. Cells were resuspended in 25 mM HEPES (pH 7.4) containing 200 μM DTPA, sonicated and used for the experiment. 1-steraoyl-2-arachidonoyl-PE was added to cell lysates (10 nmol per 3 × 10^6 cells) and incubated at 37 °C for 2 h in the absence or in the presence of human recombinant 15-LOX from *Glycine max*. In separated series of the experiment cell lysates were incubated in the presence of 1-steraoyl-2-arachidonoyl-hydroperoxy-PE (10 nmol per 3 × 10^6 cells) for 2 h at 37 °C. At the end of incubation, lipids were extracted, and oxygenated PE products were identified by MS/MS analysis using an Orbitrap Fusion Lumos mass spectrometer (Thermo Fisher Scientific). The instrument was operated with electrospray ionization probe in negative polarity mode. Ion source conditions were set as follows: spray voltage = 3 kV, sheath gas = 55 (arbitrary units), auxiliary gas = 10 (arbitrary units), sweep gas = 0.5 (arbitrary units), transfer tube temperature = 300 °C, vaporizer temperature = 200 °C, RF-lens level = 20%. Data were acquired in data-dependant-MS^2 targeted-MS^3 mode with cycle time setting of 3 s. For MS scan event, the parameters were set as follows: ion detection = orbitrap, mass resolution = 120,000, scan range = *m/z* 400–1,800, AGC target = 1× 10^5. The most intense ion was selected for the data-dependent MS^2 scan. Dynamic exclusion time was 9 s. Exclusion mass list for MS^2 (*m/z* values of 130 background ions) was created from solvent–blank injection data. For MS^2 scan event(s), the parameters were set as follows: quadrupole isolation = 1 Da, first mass = *m/z* 87, Activation type = HCD, collision energy = 28% with step 8%, ion detection = orbitrap, mass resolution = 15,000, max injection time = 250 ms, AGC target = 2 × 10^4. Product ions from a targeted mass list were selected for MS^3 scan. Target mass list for MS^3: 319.2279, 317.2123, 335.2228, 333.2072, 317.2123, 351.2159, 333.2054, 349.2003, 331.1898, 367.2126, 349.2021, 331.1916. For MS^3 scan event(s), the parameters were set as follows: top *N* = 4, isolation window = 2 Da, activation type = HCD, collision energy = 40%, ion detection = ion trap, ion trap scan rate = rapid, max injection time = 500 ms, AGC target = 3 × 10^4.

Oxygenation of SAPE and SAPC. Liposomes containing SAPE and SAPC (ratios 1:1 and 1:4) were incubated with recombinant human 15-LOX-2 (2 U/ml) in 25 mM borate buffer (pH 7.8) containing 0.003% Tween and 100 μM DTPA for 30 min at room temperature with constant oxygen bubbling. Samples were extracted with chloroform and methanol, and LC/MS analysis was performed as described above.

Determination of long-chain acyl-CoAs. Long-chain acyl-CoAs were extracted from the collected cells with chloroform–ethanol mixture[46] and then isolated with 2-(2-pyridyl) ethyl-functionalized silica gel SPE cartridges (Supelco)[47]. The contents of molecular species of long-chain acyl-CoAs were determined by LC/MS[48].

Arachidonoyl-CoA oxidation. Exhaustive oxidation of arachidonoyl-CoA by human recombinant 15-LOX-2 was performed at 21 °C for 60 min in the presence of 1.2 μM H_2O_2 plus 0.3 mM $CaCl_2$ in 25 mM HEPES buffer containing 100 μM. TPA (pH = 7.4).

LC-MS analysis of phospholipids and fatty acids. Lipids were extracted by the Folch procedure[49], and phospholipids and fatty acids were further analyzed by LC-MS/MS using normal-phase (silica) or reverse-phase (C18) chromatography followed by MS and MS/MS analysis on a Q-Exactive hybrid-quadrupole-orbitrap mass spectrometer (Thermo Fisher Scientific).

Identification of oxygenated PE in cells. PE fraction (containing both nonoxygenated and oxygenated PE (PEox)) was obtained from WT cells treated with AA and exposed to RSL3 by normal-phase LC/MS. PE and PEox (PE-OOH) were separated on a reverse-phase column (Luna 3 μm C_8 (2) 100 Å, 150 × 4.6 mm (Phenomenex). The column was maintained at room temperature. The analysis was performed using an isocratic solvent system consisting of acetonitrile/H_2O/trimethylamine/acetic acid (45:5:0.5:0.5, v/v/v/v). All solvents were LC/MS grade. The column was eluted at a flow rate of 1.5 ml/min, and the eluant was monitored by UV absorbance at 205 and 235 nm on a Shimadzu HPLC system (Shimadzu). Fractions containing PEox were collected, and identification was confirmed by mass spectrometry.

LC-MS analysis of free and esterified fatty acids. Lipids were extracted by Folch procedure[49]. Oxygenated free fatty acids were obtained from total lipids by solid-phase extraction (SPE) using OASIS HLB 1cc (30 mg) extraction cartridges (Waters Corp.) as described[50]. To liberate esterified oxygenated fatty acids, lipid extracts were treated with platelet-activating factor–acetylhydrolase (PAF-AH) (0.01 units/100 nmol of phospholipids, 45 min at 37 °C in HEPES buffer, pH 7.4). Liberated oxygenated fatty acids were extracted by SPE and analyzed by reverse-phase LC/MS (see below).

Normal-phase column separation of phospholipids. Phospholipids were separated on a normal-phase column (Luna 3 μm Silica (2) 100 Å, 150 × 2.0 mm, (Phenomenex)) at a flow rate of 0.2 mL/min on a Dionex Ultimate 3000 HPLC system. The column was maintained at 35 °C. The analysis was performed using gradient solvents (A and B) containing 10 mM ammonium acetate and 0.5% triethylamine. Solvent A contained propanol/hexane/water (285:215:5, v/v/v) and solvent B contained propanol/hexane/water (285:215:40, v/v/v). All solvents were LC/MS grade. The column was eluted for 0.5 min isocratically at 25% B, then from 0.5 to 6.5 min with a linear gradient of 25–40% solvent B, from 6.5 to 25 min using a linear gradient of 40–55% solvent B, from 25 to 38 min with a linear gradient of 55–70% solvent B, from 38 to 48 min using a linear gradient of 70–100% solvent B, then isocratically from 48 to 55 min at 100% solvent B followed by a return to initial conditions from 55 to 70 min from 100% to 25% B. The column was then equilibrated at 25% B for an additional 5 min.

Reverse-phase column separation of fatty acids. Fatty acids were separated on a reverse-phase column (Luna 3 μm C18 (2) 100 Å, 150 × 1.0 mm, (Phenomenex) at a flow rate of 0.050 mL/min). The column was maintained at 35 °C. The analysis was performed using gradient solvents (A and B) containing 10 mM ammonium acetate. Solvent A contained methanol/H_2O/acetonitrile (10:85:5, v/v/v). Solvent B contained methanol/H_2O/acetonitrile/propanol (90:5:5:0.5, v/v/v/v). All solvents were LC/MS grade. The column was eluted for 0.5 min at 50% B and from 0.5 to 2.5 min with a linear gradient of 50–75% solvent B, then isocratically from 2.5 to 10 min at 75% solvent B, from 10 to 15 min with a linear gradient of 75–100% solvent B and isocratically at 100% B for 15–20 min. At 21 min, the column was returned to starting conditions (50% solvent B) and held at this condition for an additional 9 min.

MS and MS/MS analysis of phospholipids. MS and MS/MS analysis of PLs was performed on a Q-exactive hybrid-quadrupole-orbitrap mass spectrometer (Thermo Fisher Scientific). Analysis was performed in negative ion mode at a resolution of 140,000 for the full MS scan and 17,500 for the MS^2 scan in data-dependent mode. The scan range for MS analysis was 400–1,800 *m/z* with a maximum injection time of 128 ms using 1 microscan. A maximum injection time of 500 ms was used for MS^2 (high-energy collisional dissociation (HCD))

doi:10.1038/nchembio.2238

analysis with collision energy set to 24 with an inclusion list for phospholipids including PE, PC and CL and their oxidized and deuterated products. An isolation window of 1.0 Da was set for the MS and MS^2 scans. Capillary spray voltage was set at 3.5 kV, and capillary temperature was 320 OC. The S-lens Rf level was set to 60.

MS and MS/MS analysis of fatty acids. MS and MS/MS analysis of PLs was performed on a Q-exactive hybrid-quadrupole-orbitrap mass spectrometer (Thermo Fisher Scientific). Analysis was performed in negative ion mode at a resolution of 140,000 for the full MS scan and 17,500 for the MS^2 scan in data-dependent mode. The scan range for MS analysis was 150–500 *m/z* with a maximum injection time of 100 ms using 1 microscan. A maximum injection time of 100 ms was used for MS^2 (high-energy collisional dissociation (HCD)) analysis, with collision energy set to 30 and an inclusion list for fatty acids, fatty acid metabolites and their oxidized and deuterated products. An isolation window of 1.0 Da was set for the MS and MS^2 scans. Capillary spray voltage was set at 3.2 kV, and capillary temperature was 320 OC. The S-lens Rf level was set to 65.

Detection of tocopherols and oxidized AA by LC/MS. *Reaction conditions.* 20 μM AA was incubated at 37 °C with 2.8 mU of 15-LOX and 10 μM of each inhibitor in 50 mM Tris-HCl buffer (pH 7.4) for 5 min. The reactions were stopped by adding a nine-fold excess of acetonitrile. For oxidized AA analysis, 1 μM internal standard was added to the above mixture and analyzed through LC-MS as described previously[51]. Vitamin E was extracted by Folch procedure[49], and LC-ESI-MS analysis was performed on a Dionex LC system (UltiMate 3000 autosampler) coupled to an LXQ ion trap mass spectrometer with the Xcalibur operating system, (Thermo Fisher Scientific). The instrument was operated in positive ion mode at 5.0 kV. The source temperature was maintained at 175 °C. Spectra were acquired using full range zoom (*m/z* 200–600) scans. Tocopherol and its analogs were separated on a reverse-phase column Luna 3 μm C18 (2) 100 Å, 150 mm × 1 mm (Phenomenex) at a flow rate of 0.065 mL/min. The column was maintained at 30 °C. The analysis was performed using gradient solvents (A and B). Solvent A consisted methanol/water (1:1) containing 5 mM ammonium acetate. Solvent B consisted of methanol containing 0.1% NH_4. The column was eluted during the first 5 min isocratically at 65% solvent B, from 5 to 10 min with a linear gradient from 65% to 95% solvent B, from 10 to 20 min with a linear gradient from 95% to 100%, from 20 to 25 min isocratically using 100% solvent B, from 25 to 30 min with a linear gradient from 100% to 65% solvent B, and from 30 to 35 min isocratically using 65% solvent B for equilibration of the column.

Detection of tocopherol phenoxyl radicals by ESR spectroscopy. Reaction conditions and ESR spectrometer settings: ESR spectrometer (JEOL JES-FA100) settings were center field 335.5 mT, scan range 10 mT, scan sweep 10 mT/min (10 scans), time constant 0.1 s, magnetic field 100 kHz, modulation amplitude 0.2 mT, microwave frequency 9.44 GHz, microwave power 50 mW, receiver gain 5×10^3 and at 25 °C. Phenoxyl radicals of α-tocopherol and its analogs (3 mM) were generated by 15-LOX (2.5 KU) in the presence of arachidonic acid (1 mM) in PBS pH 7.4, deoxycholic acid sodium salt (0.1%) and DTPA (100 μM).

Molecular docking. Molecular docking modeling was employed to study the interactions of free and esterified fatty acids and vitamin E family molecules with human 15-LOX-2 (PDB 4NRE)[52]. The small molecules—lipids or inhibitors—were docked to the proteins using AutoDock Vina program, version 1.1.2 (http://vina.scripps.edu). The lipids, inhibitors and protein structures were converted from Protein Data Bank into PDBQT format using MGL Tools (http://mgltools.scripps.edu). Owing the large size of 15-LOX-2 protein, we applied a large grid box for the docking modeling. We used grid boxes with dimensions of 112 × 102 × 72 Å. Three docking models were run using three random number generator seeds, with the exhaustiveness set at 14 to obtain a higher accuracy in finding the binding site and reduce the discrepancies among binding affinities. From these we selected the best model, in which the small molecule was bound at the catalytic site of 15-LOX-2 with the highest binding affinity (the lowest binding energy).

Coarse-grained molecular dynamics (CGMD) simulations. CGMD simulations were based on the MARTINI force field for biomolecular simulations[53]. CGMD simulations were applied to study the interactions of 15-LOX-2 with the membrane comprised of PC and PE. The protein was located ~20 Å from the membrane surface, with different orientations. The position of protein was restricted during equilibration runs. A 15-fs time step was used to integrate the equations of motion. Analysis of the final configuration of the CGMD runs revealed the preferred phospholipid substrate. All simulations were performed using the GROMACS v. 4.5.4 MD package[54] and visualized using VMD v. 1.9 software (http://www.ks.uiuc.edu/Research/vmd/). Initially, each system was minimized for 20 ps, before 1 ns NVT and 1 ns NPT ensemble equilibration. A 15-fs time step was used to integrate the equations of motion. Nonbonded interactions have a cutoff distance of 1.2 nm. Simulations were run at 310 K and at 1 atm during NPT runs.

Mathematical modeling. We constructed the phospholipid metabolic network regulating ferroptosis based on data presented in this manuscript, published in the literature[55,56] or found in the Reactome and KEGG databases. The reaction scheme of the network is shown in **Supplementary Figure 16a**. All acronyms used are defined in **Supplementary Table 3**. A system of ODEs derived from the reaction network is described below. Simulations and sensitivity analysis were performed using COPASI[57] with the LSODA solver.

Here we briefly describe the three modules in our network model:

1. AA metabolism: the release of AA from membrane phospholipids can be catalyzed by enzymes such as PLA2. The free AA is oxidized to 5-HPETE, 12-HPETE and 15-HPETE (referred to collectively below as 5/12/15-HPETE) by 5-LOX, 12-LOX and 15-LOX, respectively, which are reduced to 5-HETE, 12-HETE and 15-HETE (below 5/12/15-HETE), respectively, by GPX4 in the presence of GSH. 5-LOX further converts 5-HETE into LTA_4. AA is also oxidized by COX to produce PGH_2, which leads to the production of lipid mediators including PGE2. The feedback reactions involving 5/12/15-HPETE, 5/12/15-HETE, LTA_4 and PGE_2 were based on the literature[55,56].

2. AA-induced ferroptosis: Acsl4 catalyzes the formation of AA-CoA. Elongase elongates AA-CoA to AdA-CoA. AA-CoA and AdA-CoA can be broken down via β-oxidation or esterified into PE to form PE-AA and PE-AdA in a reaction catalyzed by Lcat3. LOXes convert PE-AA and PE-AdA into PE-AA-OOH and PE-AdA-OOH, respectively. The accumulation of PE-AA-OOH and PE-AdA-OOH leads to ferroptotic cell death.

3. GPX4-dependent regulation: system x_c^- imports cysteine and exports glutamic acid. GCS catalyzes the formation of cysteine–glutamic acid, which reacts with glycine and forms GSH in a reaction catalyzed by GS. GSH is converted into GSSG by GPX4, while PE-AA-OOH and PE-AdA-OOH are reduced into PE-AA-OH and PE-AdA-OH. GR catalyzes the conversion from GSSG to GSH.

The dynamics of the network was modeled as a system of 47 ordinary differential equations (ODEs) (**Supplementary Table 4**). The reaction rates for catalysis are described using Michaelis–Menten kinetics. For example, for an enzyme catalytic reaction described by

$$S + E \xrightarrow{v} P + E$$

S denotes substrate, *E* denotes enzyme, *P* denotes product, and *v* is the reaction rate. The kinetics of the reaction is modeled as

$$v = \frac{K_{cat} \cdot S \cdot E}{K_m + S}$$

where K_{cat} is the turnover number and K_m is the Michaelis–Menten constant. The rate equation for catalysis involving two substrates, S_1 and S_2, is

$$v = \frac{K_{cat} \cdot S_1 \cdot S_2 \cdot E}{K_{m1} \cdot K_{m2} + K_{m1} \cdot S_1 \cdot K_{m2} \cdot S_2 + S_1 \cdot S_2}$$

The rate equation for the catalysis involving inhibitors I_1, I_2, … is

$$v = \frac{K_{cat} \cdot S \cdot E}{K_m(1 + \frac{I_1}{K_{i1}} + \frac{I_2}{K_{i2}} + \ldots) + S}$$

The rate equation for the catalysis involving activators A_1, A_2, … is

$$v = \frac{K_{cat} \cdot S \cdot E \cdot (1 + \frac{A_1}{K_{a1}} + \frac{A_2}{K_{a2}} + \ldots)}{K_m + S_2}$$

The reaction rates for transcriptional regulation and decay are modeled using a Hill equation and mass law kinetics, respectively.

We defined a score indicating cell death signal strength as a linear combination of the concentrations of PE-AA-OOH and PE-AdA-OOH:

$$S_{death} = \alpha + \beta_1 \cdot [PE - AA - OOH] + \beta_2 \cdot [PE - AdA - OOH]$$

where α is the basal level of cell death, and β_1 and β_2 are coefficients. We then use the integration of S_{death} over time to predict cell death level (percentage).

We used the experimental data obtained to calibrate model parameters including initial concentrations of species and reaction rate constants. Specifically, we used the data shown in **Figure 1c** to establish the relationship between RSL3 pretreatment time and initial concentration of GPX4. We then estimated the unknown parameters by fitting the experimental data of ferroptotic cell death levels under different conditions. The model was further validated using an independent test data set. The comparison and model predictions and experimental data are shown in **Supplementary Figure 16b–i**. The resulting parameters are shown in **Supplementary Table 5**.

Statistical analysis. Data are presented as mean ± s.d. from at least three experiments unless otherwise specified. Statistical analyses were performed by either unpaired Student's *t*-test or one-way ANOVA. The threshold of significance was set at $P < 0.05$. Phospholipids were quantified from full-scan LC/MS spectra with ratiometric comparison to the preselected internal standard using a corresponding standard curve for each phospholipid class. Differences between the groups were analyzed by one-way ANOVA with Tukey's *post hoc* analyses by SPSS 18.0 software (SPSS Inc). Orthogonal partial least-squares discriminant analysis (OPLS-DA) was used to discriminate between live and ferroptotic cells using SIMCA 13.0 software (Umetrics). The criteria for confirming a potential biomarker were: (i) variable importance in projection (VIP) greater than 1, (ii) jack-knife uncertainty bar excluding 0 and (iii) absolute value of Pcorr in the S-plot greater than 0.58.

44. Telmer, C.A. *et al.* Rapid, specific, no-wash, far-red fluorogen activation in subcellular compartments by targeted fluorogen activating proteins. *ACS Chem. Biol.* **10**, 1239–1246 (2015).
45. Szent-Gyorgyi, C. *et al.* Fluorogen-activating single-chain antibodies for imaging cell surface proteins. *Nat. Biotechnol.* **26**, 235–240 (2008).
46. Tardi, P.G., Mukherjee, J.J. & Choy, P.C. The quantitation of long-chain acyl-CoA in mammalian tissue. *Lipids* **27**, 65–67 (1992).
47. Minkler, P.E., Kerner, J., Ingalls, S.T. & Hoppel, C.L. Novel isolation procedure for short-, medium-, and long-chain acyl–coenzyme A esters from tissue. *Anal. Biochem.* **376**, 275–276 (2008).
48. Sun, D., Cree, M.G. & Wolfe, R.R. Quantification of the concentration and ^{13}C tracer enrichment of long-chain fatty acyl–coenzyme A in muscle by liquid chromatography/mass spectrometry. *Anal. Biochem.* **349**, 87–95 (2006).
49. Folch, J., Lees, M. & Sloane Stanley, G.H. A simple method for the isolation and purification of total lipides from animal tissues. *J. Biol. Chem.* **226**, 497–509 (1957).
50. Miller, T.M. *et al.* Rapid, simultaneous quantitation of mono and dioxygenated metabolites of arachidonic acid in human CSF and rat brain. *J. Chromatogr. B Analyt. Technol. Biomed. Life Sci.* **877**, 3991–4000 (2009).
51. Tejero, J. *et al.* Peroxidase activation of cytoglobin by anionic phospholipids: mechanisms and consequences. *Biochim. Biophys. Acta* **1861**, 391–401 (2016).
52. Kobe, M.J., Neau, D.B., Mitchell, C.E., Bartlett, S.G. & Newcomer, M.E. The structure of human 15-lipoxygenase-2 with a substrate mimic. *J. Biol. Chem.* **289**, 8562–8569 (2014).
53. Marrink, S.J., Risselada, H.J., Yefimov, S., Tieleman, D.P. & de Vries, A.H. The MARTINI force field: coarse grained model for biomolecular simulations. *J. Phys. Chem. B* **111**, 7812–7824 (2007).
54. Van Der Spoel, D. *et al.* GROMACS: fast, flexible, and free. *J. Comput. Chem.* **26**, 1701–1718 (2005).
55. Yang, K. *et al.* Dynamic simulations on the arachidonic acid metabolic network. *PLoS Comput. Biol.* **3**, e55 (2007).
56. Gupta, S., Maurya, M.R., Stephens, D.L., Dennis, E.A. & Subramaniam, S. An integrated model of eicosanoid metabolism and signaling based on lipidomics flux analysis. *Biophys. J.* **96**, 4542–4551 (2009).
57. Hoops, S. *et al.* COPASI—a COmplex PAthway SImulator. *Bioinformatics* **22**, 3067–3074 (2006).

doi:10.1038/nchembio.2238